Journal of Medicinal Chemistry

Article

pubs.acs.org/jmc

Exploration of Allosteric Agonism Structure−Activity Relationships within an Acetylene Series of Metabotropic Glutamate Receptor 5 ($mGlu_5$) Positive Allosteric Modulators (PAMs): Discovery of 5-((3-Fluorophenyl)ethynyl)-*N*-(3-methyloxetan-3-yl)picolinamide (ML254)

Mark Turlington,[†,‡,§] Meredith J. Noetzel,[†,‡] Aspen Chun,[†,‡,§] Ya Zhou,[†,‡,§] Rocco D. Gogliotti,[†,‡,§] Elizabeth D. Nguyen,[¶] Karen J. Gregory,[†,‡,⊥] Paige N. Vinson,[†,‡] Jerri M. Rook,[†,‡] Kiran K. Gogi,[†,‡] Zixiu Xiang,[†,‡] Thomas M. Bridges,[†,‡,§] J. Scott Daniels,[†,‡,§] Carrie Jones,[†,‡,§] Colleen M. Niswender,[†,‡,§] Jens Meiler,[†,∥,¶,#] P. Jeffrey Conn,[†,‡,§] Craig W. Lindsley,[†,‡,§,∥] and Shaun R. Stauffer*[,†,‡,§,∥]

[†]Department of Pharmacology, [‡]Vanderbilt Center for Neuroscience Drug Discovery, [¶]Center for Structural Biology, and [#]Vanderbilt Institute for Chemical Biology, Vanderbilt University Medical Center, Nashville, Tennessee 37232, United States

[§]Vanderbilt Specialized Chemistry Center for Probe Development (MLPCN), Nashville, Tennessee 37232, United States

[∥]Department of Chemistry, Vanderbilt University, Nashville, Tennessee 37232, United States

[⊥]Drug Discovery Biology, Monash Institute of Pharmaceutical Sciences, Monash University, Parkville, VIC 3052, Australia

Supporting Information

ABSTRACT: Positive allosteric modulators (PAMs) of metabotropic glutamate receptor 5 ($mGlu_5$) represent a promising therapeutic strategy for the treatment of schizophrenia. Both allosteric agonism and high glutamate fold-shift have been implicated in the neurotoxic profile of some $mGlu_5$ PAMs; however, these hypotheses remain to be adequately addressed. To develop tool compounds to probe these hypotheses, the structure−activity relationship of allosteric agonism was examined within an acetylenic series of $mGlu_5$ PAMs exhibiting allosteric agonism in addition to positive allosteric modulation (ago-PAMs). PAM **38t**, a low glutamate fold-shift allosteric ligand (maximum fold-shift ∼3.0), was selected as a potent PAM with no agonism in the in vitro system used for compound characterization and in two native electrophysiological systems using rat hippocampal slices. PAM **38t** (ML254) will be useful to probe the relative contribution of cooperativity and allosteric agonism to the adverse effect liability and neurotoxicity associated with this class of $mGlu_5$ PAMs.

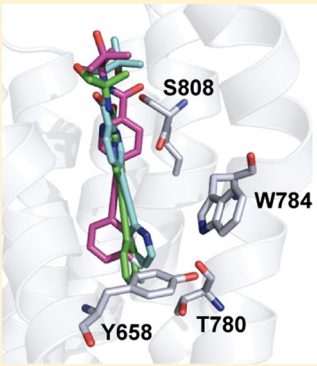

INTRODUCTION

A largely unmet medical need affecting approximately 1% of the world's population, schizophrenia is a complex mental illness characterized by three symptom clusters including positive symptoms (hallucinations, paranoia, disorganized behavior), negative symptoms (social withdrawal, anhedonia, flat affect), and cognitive dysfunction (deficits in attention, learning, and memory).[1−4] Current treatments for schizophrenia were developed based on the dopaminergic hypothesis of schizophrenia, which points to overactivation of subcortical dopamine D_2 receptors as a causative factor for the positive symptoms of the disease.[5,6] Accordingly, first-generation typical antipsychotics (e.g., haloperidol) act as D_2 antagonists, and second-generation atypical antipsychotics (e.g., clozapine, risperidone) act as mixed D_2/5-HT_{2A} antagonists, as well as having activity at other receptors.[5,6] Both classes are routinely used to treat the positive symptoms of schizophrenia, and several statistical analyses have revealed that there is little evidence for improved efficacy of atypical over typical antipsychotics except in severe cases of schizophrenia.[7,8] However, the two classes are different in their side-effect profiles. Whereas typical antipsychotics are plagued by extra-pyramidal side effects (movement disorders), atypical antipsychotics often offer improved side-effect profiles but are associated with significant weight gain.[8] In addition to the considerable adverse effect profiles, neither class of antipsychotics has a substantial impact on the negative and cognitive symptoms of the disorder, and 20% of patients are nonresponsive to treatment.[1] These severe limitations highlight the need to develop new treatments for schizophrenia.

In addition to the dopaminergic pathways, disruptions in many neuronal circuits including the glutamatergic, GABAergic, and cholinergic pathways are observed in schizophrenic patients.[3] Importantly, abnormalities in glutamatergic circuits have been linked with all three symptom clusters of schizophrenia, fueling the development of the glutamate hypothesis of schizophrenia as a means to address all symptom clusters. Clinical observations have revealed that phenylcyclidene (PCP) and ketamine, antagonists of the ionotropic *N*-methyl-D-aspartate glutamate receptor (NMDAR), produce

Received: July 8, 2013
Published: September 19, 2013

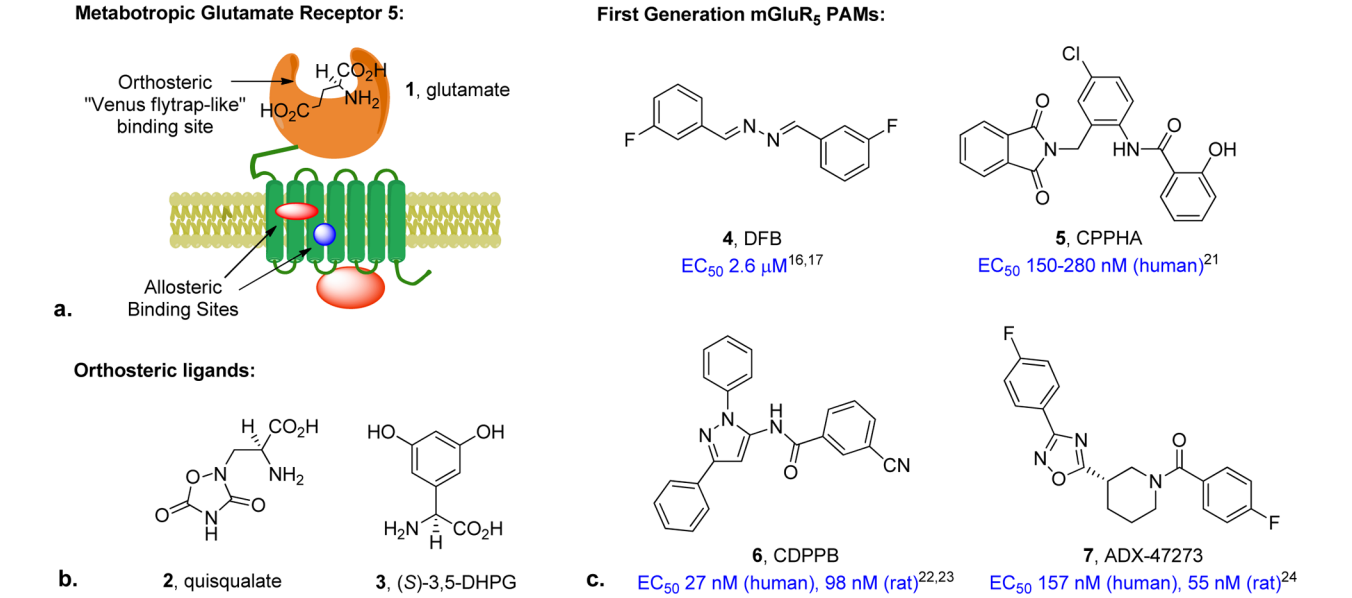

Figure 1. (a) Representative $mGlu_5$ receptor (protomer of dimer) with orthosteric and allosteric binding sites. (b) Orthosteric $mGlu_5$ ligands. (c) First generation $mGlu_5$ PAMs.

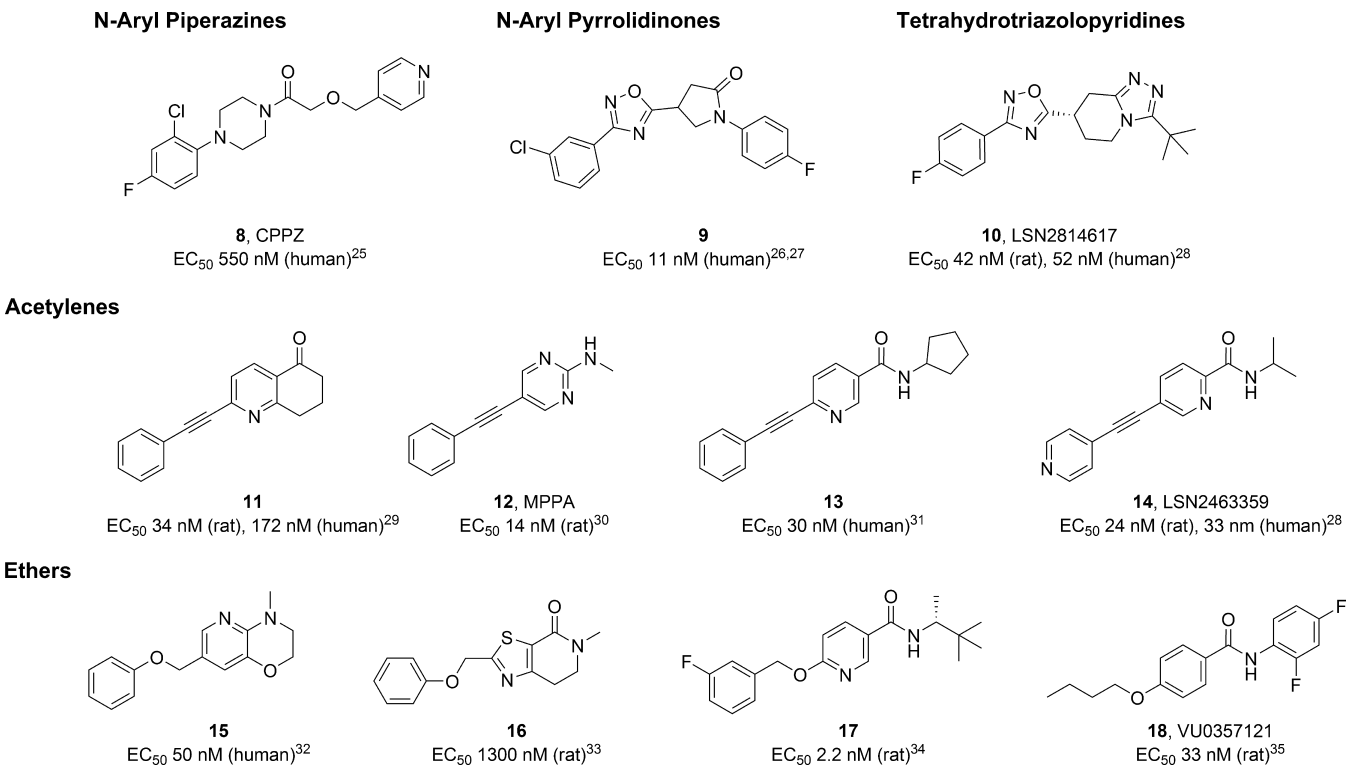

Figure 2. $mGlu_5$ PAM chemotypes and reported PAM potencies.

schizophrenic-like symptoms.[1−4,9−13] Furthermore, administration of high doses of the NMDA co-agonists glycine, D-serine, and D-cycloserine improves positive, negative, and cognitive symptoms in schizophrenic patients,[1,2,14,15] generating excitement that enhancement of glutamatergic neurotransmission could be a novel strategy for the treatment of schizophrenic symptoms. While direct activation of NMDAR results in toxicity associated with ion channel overactivation,[1,2] the metabotropic glutamate receptor 5 ($mGlu_5$) is closely associated with NMDAR function and may provide an indirect means to rescue NMDAR hypofunction with a lower propensity for toxicity. Numerous studies indicate that $mGlu_5$ plays a critical role in modulating neurotransmission in forebrain circuits implicated in NMDAR antagonist mediated psychotomimetic effects, and the ability to more subtly modulate NMDAR activity has been proposed to result in a potentially lower propensity for toxicity.[1,2,4,13,16,17]

$mGlu_5$ is a member of the Family C G protein-coupled receptors (GPCRs) that bear a large extracellular "Venus flytrap-like" domain that serves as the binding site for glutamate. The high sequence homology of the glutamate binding sites among the eight known metabotropic glutamate

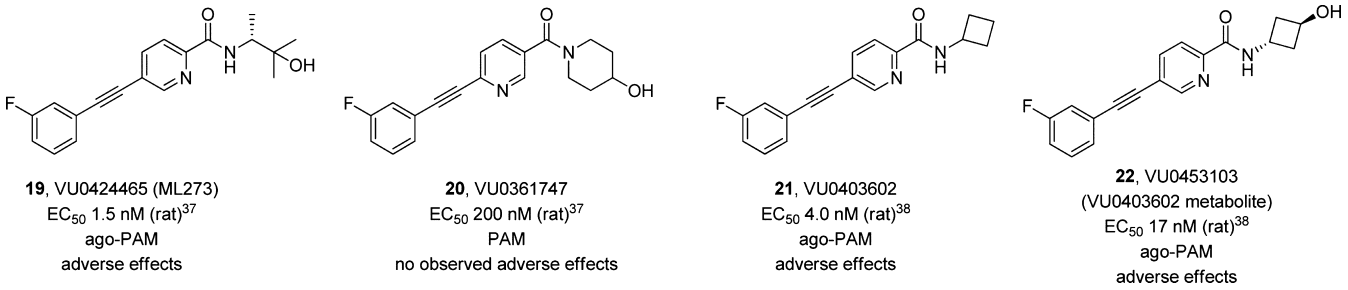

Figure 3. Acetylene $mGlu_5$ PAMs used to assess seizure activity in animal models.[37,38]

receptor (mGlu) subtypes has made the development of subtype selective $mGlu_5$ orthosteric agonists difficult.[2,4] In contrast, spatially distinct allosteric binding sites that reside in the transmembrane domain of the receptor (Figure 1) possess less sequence conservation across the mGlu subtypes, making possible the discovery of $mGlu_5$ selective ligands. Allosteric ligands can activate the receptor directly (allosteric agonists) or can modulate the activity of the receptor in the presence of the endogenous ligand glutamate, either enhancing (positive allosteric modulators, PAMs) or diminishing (negative allosteric modulators, NAMs) receptor activity.[18−20] Allosteric modulators with no agonist activity may provide a more subtle and physiologically relevant approach to restoring target function in comparison to orthosteric/allosteric agonists as receptor response occurs only in the presence of the endogenous agonist.[18−20] In addition, allosteric modulators often offer improvements in chemical tractability and improved properties for central nervous system (CNS) exposure over traditional orthosteric glutamate analogues such as quisqualate and (*S*)-3,5-DHPG, which have difficulty passing the blood−brain barrier.[16,18−20]

The advantages of allosteric modulators have fueled the development of highly subtype-selective and CNS-penetrant $mGlu_5$ PAMs.[16,17,21] The earliest $mGlu_5$ PAMs are represented by the four chemotypes shown in Figure 1. 3,3′-Difluorobenzaldazine (DFB), developed by Merck & Co. in 2003, represented the first subtype-selective $mGlu_5$ PAM, and the ensuing discovery of *N*-(4-chloro-2-((1,3-dioxoisoindolin-2-yl)methyl)phenyl)-2-hydroxybenzamide (CPPHA) in 2004 provided a compound with improved potency and properties suitable for use in native preparations.[21] Shortly thereafter, the first highly useful in vivo tool compound, 3-cyano-*N*-(1,3-diphenyl-1*H*-pyrazol-5-yl)benzamide (CDPPB) was discovered by Merck scientists,[22,23] and researchers at Addex Pharmaceuticals reported a chemically distinct $mGlu_5$ PAM, ADX-47273 (**7**), with suitable properties for in vivo studies.[24] Utilizing these compounds, studies in animal models have added evidence to the promise of $mGlu_5$ allosteric activation as a novel therapeutic strategy for the treatment of schizophrenia. PAM **6** has been shown to possess efficacy in animal models predictive of positive symptoms (amphetamine-induced hyperlocomotion (AHL), prepulse inhibition of acoustic startle reflex), cognitive deficits (behavioral and cognitive flexibility, Morris water maze (MWM)), and negative symptoms (sucrose preference).[16,22,23,36] Studies with **7** have revealed similar efficacy in reversal of positive symptoms (conditioned avoidance responding, apomorphine-induced climbing, AHL) and improvements in cognition (novel object recognition, five-choice serial reaction time test, MWM).[16,24,36] In the wake of these studies, numerous novel $mGlu_5$ PAM chemotypes have been discovered and optimized, leading to improvements in potency and physiochemical properties.[16,17] Representatives of major chemotypes are shown in Figure 2, and many of these compounds have demonstrated efficacy in antipsychotic and cognition models.[25−36] In addition, Lilly recently revealed $mGlu_5$ PAMs LSN2814617 (**10**) and LSN2463359 (**14**).[28] Both **10** and **14** are reported to shift a concentration−response curve for the group I orthosteric agonist, DHPG, in rat cortical neurons with relatively weak efficacies compared to historical $mGlu_5$ PAMs (**10**, FS = 2.8 at 3 μM; **14**, FS = 2.0 at 1 μM). In vivo, these compounds have been reported to exert significant effects in multiple models including the methylazoxymethanol (MAM) neurodevelopmental model of schizophrenia, wake-promoting properties in acute sleep-wake electroencephalogram (EEG), and reversal of NMDAR antagonist SDZ 220,581-induced disruptions in delayed-matching-to-position (DMTP).[28] Interestingly, these low efficacy PAMs do not substantially impact baseline performance on their own in DMTP, nor do they have significant effects in reversal of hyperlocomotion in the AHL model, which is in contrast to previously reported $mGlu_5$ PAMs that maintain higher efficacies (orthosteric agonist concentration−response curve EC_{50} fold-shift greater than 3.0).[17,23−25,30,33,36]

Despite the therapeutic promise of $mGlu_5$ PAMs, recent findings have begun to reveal a CNS adverse-effect (AE) liability for certain classes of $mGlu_5$ PAMs.[37−39] The seizure-inducing effects of group I mGlu *orthosteric* agonists is well-known;[40,41] however, the potential for mechanism-related AEs associated with *allosteric* $mGlu_5$ receptor activation was not appreciated until recently. Studies in our laboratories have demonstrated that allosteric modulator **19** (VU0424465, ML273, Figure 3) causes seizure activity in rodents.[37] This effect can be blocked by treatment with 2-methyl-6-(2-phenylethynyl) pyridine (MPEP), an allosteric $mGlu_5$ NAM, pointing to the role of $mGlu_5$ in the observed neurotoxicity. Our recombinant $mGlu_5$ cell line with low receptor density is predicted to have a better correlation with the functional response observed in native systems and thus serves as a more definitive assay system to detect allosteric agonism.[43] Allosteric modulator **19** displays both allosteric agonism and PAM activity (ago-PAM activity) in a $mGlu_5$ cell line with low receptor density, as well as in native systems such as astrocytes.[37] In contrast, nicotinamide acetylene allosteric modulator **20** (VU0361747, Figure 3) was devoid of agonism in these low-expressing $mGlu_5$ cells and did not display a seizure liability in vivo.[37] Thus, allosteric agonist activation of $mGlu_5$, similar to orthosteric activation, can contribute to an AE liability in vivo and epileptogenesis in native systems. Further evidence in support of this hypothesis surfaced from profiling of **21** (VU0403602, Figure 3). Similarly to ago-PAM **19**, picolinamide acetylene **21** demonstrates agonist activity in a $mGlu_5$ low-expressing cell line and native systems and possesses

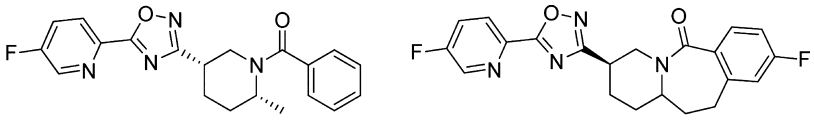

23, 5PAM523
Therapeutic Index: 2
Fold-shift: 11

24, 5PAM916
Therapeutic Index: 18
Fold-shift: 6

Figure 4. Merck-Addex compounds found to induce neurotoxicity.[39]

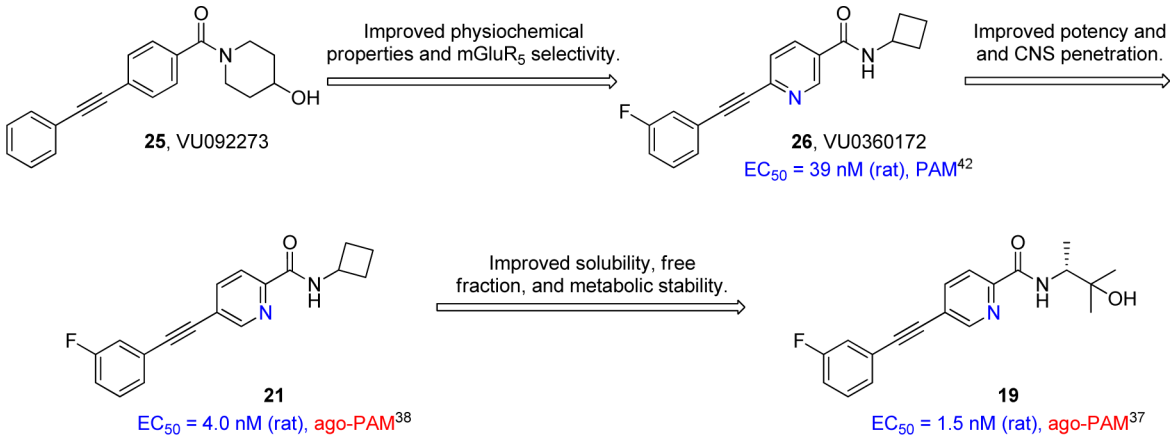

Figure 5. SAR development of Vanderbilt acetylene $mGlu_5$ PAMs. Potency values refer to the low density rat $mGlu_5$ receptor cell line.[43]

a seizure liability in animal models.[38] Further complicating the pharmacological effects of **21**, its principle in vivo metabolite **22** (VU0453103) also displays significant ago-PAM activity, suggesting that formation of active metabolites is possible and may contribute to an adverse effect profile in vivo. These findings highlight the need to avoid an ago-PAM pharmacological profile in both the parent compound and its major metabolites in the quest to develop allosteric ligands for $mGlu_5$ receptor activation.

Concurrent with these findings, a collaborative effort between Merck and Addex Pharmaceuticals revealed that $mGlu_5$ PAMs within their piperidine and caprolactam chemotypes induced significant convulsions and neuronal cell death in mice (Figure 4).[39] In contrast $mGlu_5$ knockout mice that were administered the compounds did not display these adverse effects. These compounds did not possess ago-PAM activity in astrocytes, suggesting allosteric agonism is not necessarily required to induce adverse effects, although the pharmacological profile of the major metabolites was not reported. While the most toxic compound reported, 5PAM523 (**23**, Figure 4), had a therapeutic index of just 2-fold (C_{max} minimum active dose amphetamine-induced hyperlocomotion versus C_{max} minimum adverse effect dose), higher therapeutic indices were observed for the additional compounds reported. Of these, 5PAM916 (**24**) was found to have the highest therapeutic index (18-fold) and the lowest glutamate EC_{50} fold-shift (6-fold at 10 μM). These observations suggest that the efficacy to shift a glutamate concentration−response curve, or more precisely, PAM cooperativity, may play an important role in neurotoxicity, such that improved safety margins may be realized by designing compounds possessing lower cooperativity.[39]

These reports, along with the adverse effect liability of allosteric agonism observed in our laboratories, suggest that PAMs devoid of agonism in situations where $mGlu_5$ expression is low and possessing moderate to low efficacy may be preferable for developing compounds with optimal safety margins. To further investigate the safety implications of ago-PAM pharmacology, we initiated medicinal chemistry efforts to explore the structural determinants of ago-PAM activity in the acetylene scaffold **19**.[37] We targeted the development of highly potent (≤10 nM) tool compounds structurally similar to **19** that did not exhibit allosteric agonism in our in vitro assay systems. In addition, the glutamate fold-shift profile of promising pure PAMs was also investigated as an indicator of cooperativity. Herein we report a detailed structure−activity relationship (SAR) of allosteric agonism within this class of acetylene-based $mGlu_5$ PAMs. This study led to the optimization and characterization of low cooperativity PAM acetylenes that possess in vitro pharmacological and pharmacokinetic profiles that will enable further studies to address ongoing questions concerning the therapeutic index of $mGlu_5$.

■ RESULTS AND DISCUSSION

Structure−Activity Relationship (SAR) Design. Our development of acetylenic $mGlu_5$ PAMs originated with a high throughput screen (HTS) lead VU0092273 (**25**, Figure 5) that was quickly optimized to the nicotinamide analogue, VU0360172 (**26**, Figure 5).[42] The introduction of the central pyridyl ring in **26** enabled salt formation leading to improved water solubility and the first orally active acetylene $mGlu_5$ PAM, despite a high degree of plasma protein binding (98.9%) and low CNS exposure (brain to plasma ratio = 0.13). Subsequent efforts to improve physiochemical properties within this class led to the discovery that picolinamide analogues, as represented by **21** (Figure 5),[38] which show a general improvement in potency, however still possess a high degree of plasma protein binding (>99% bound in human and rat). Both **21** and **26** were found to undergo substantial oxidative metabolism of the eastern cyclobutane ring (see Figure 3).[38] With these findings

Scheme 1. Synthesis of (*R*)-3-Amino-2-methylbutan-2-ol[a]

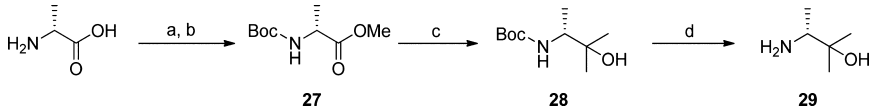

[a]Reagents and conditions: (a) $SOCl_2$, MeOH, 0 °C to rt; (b) Boc_2O, Et_3N, CH_2Cl_2, 0 °C to rt, 88% over 2 steps; (c) MeMgBr (3.0 equiv), THF, 0 °C to rt, 63%; (d) TFA/CH_2Cl_2 (1:2), 0 °C, 97%.

Scheme 2. Synthesis of Western Aryl Analogues[a]

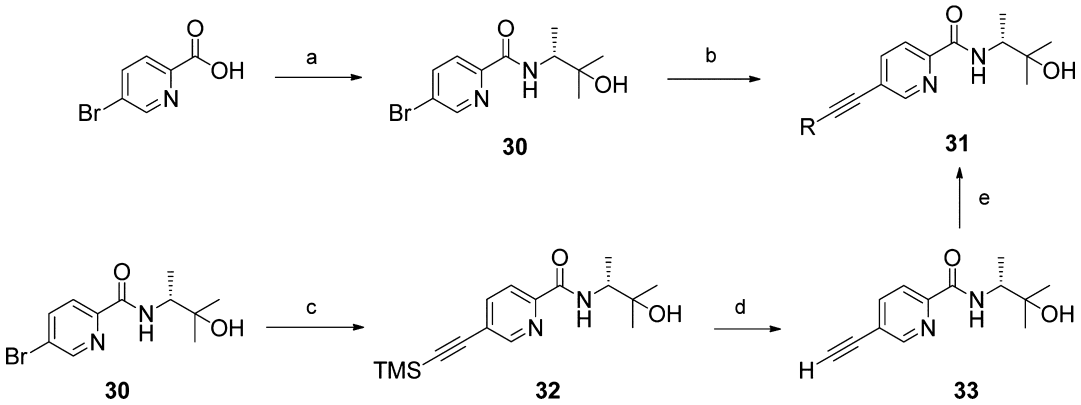

[a]Reagents and conditions: (a) **29**, HATU, DIPEA, DMF, rt, 81%; (b) terminal acetylene, CuI, $PdCl_2(PPh_3)_2$, Et_2NH, DMF, 90 °C, 50–90%; (c) trimethylsilylacetylene, CuI, $PdCl_2(PPh_3)_2$, Et_2NH, DMF, 90 °C, 77%; (d) K_2CO_3, MeOH/THF, rt, 95%; (e) aryl bromide, CuI, $PdCl_2(PPh_3)_2$, Et_2NH, DMF, 90 °C, 43–62%.

Scheme 3. Synthesis of Core Analogues[a]

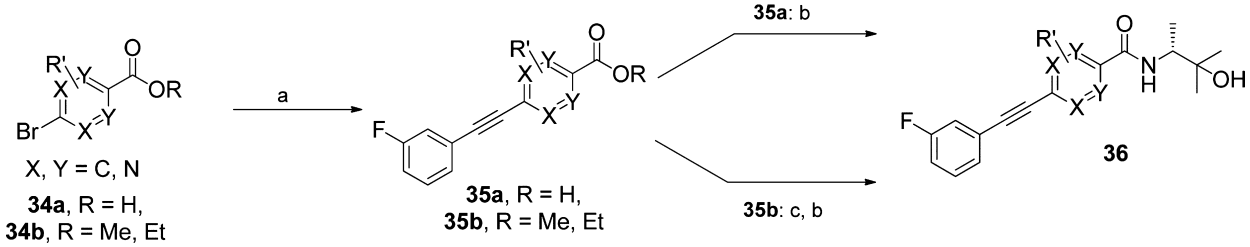

[a]Reagents and conditions: (a) 1-ethynyl-3-fluorobenzene, CuI, $PdCl_2(PPh_3)_2$, Et_2NH, DMF, 90 °C, 30–97%; (b) **29**, HATU, DIPEA, DMF, rt, (c) LiOH, THF/H_2O, rt.

we turned our efforts toward reducing lipophilicity and addressing metabolism of the eastern alkyl group through the introduction of functional groups bearing additional hydrogen bond donors and/or acceptors in this portion of the molecule. This effort led to the discovery of **19** bearing a tertiary carbinol, which contributed to improved solubility, reduced metabolism, and reduced plasma protein binding (2.8% bound in rat, 2.7% bound in human).

As **19** represented one of the first compounds within the acetylene class to possess ago-PAM activity in the low-expressing receptor cell line,[37] we initiated exploration of SAR around this analogue to probe the structural determinants of allosteric agonism. Analysis of **19** yielded three important structural features to explore: the western aryl ring, the heteroaryl core, and the eastern amide region. The western aryl ring was hypothesized to be a structural region that might impact in vitro PAM to NAM profile mode switching as observed in related acetylenes.[17] The importance of the core region was suggested by the fact that nicotinamide containing acetylenes **26** and **20** were active as PAMs but devoid of agonist activity (Figures 3 and 5). Lastly, the hydroxyl motif in the eastern amide region of **19** and metabolite **22**[38] was identified as a common structural motif among acetylenes possessing adverse effect profiles; therefore, alternate functional groups designed to maintain good pharmacokinetic and physiochemical properties were targeted.

Chemistry. To explore western aryl and core analogues (*R*)-3-amino-2-methylbutan-2-ol, **29**, was first prepared as shown in Scheme 1.[34] Starting from D-alanine, the amino acid was transformed into the methyl ester upon treatment with $SOCl_2$ in MeOH. Protection of the amine as the *tert*-butyl carbamate yielded intermediate **27** in 88% yield over the 2 steps. Reaction with MeMgBr (3.0 equiv) yielded tertiary alcohol **28** in 63% yield, and deprotection in the presence of TFA/CH_2Cl_2 afforded (*R*)-3-amino-2-methylbutan-2-ol, **29**. While the amino alcohol could be stored as the TFA salt and used over a period of several weeks, best results were obtained by removing the *tert*-butyl carbamate immediately prior to use.

The desired analogues to explore the structural properties of compounds possessing allosteric agonism were accessed in the parallel synthetic sequences shown in Schemes 2–4. The western aryl region was rapidly diversified utilizing key

Scheme 4. Synthesis of Eastern Amide Analogues[a]

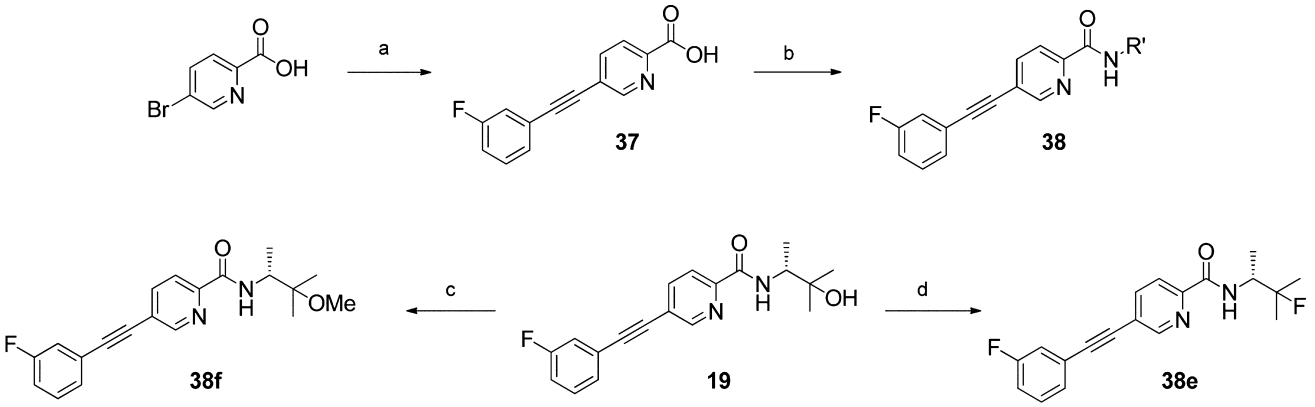

[a]Reagents and conditions: (a) 1-ethynyl-3-fluorobenzene, CuI, $PdCl_2(PPh_3)_2$, Et_2NH, DMF, 90 °C, 65%; (b) amine, HATU, DIPEA, DMF, rt; (c) NaH, MeI, THF, 0 °C to rt, 58%; (d) DAST, CH_2Cl_2, −78 °C to rt, 30%.

intermediates **30** and **33**. 5-Bromo-picolinamide **30** was accessed via a HATU-mediated amide coupling of 5-bromopicolinic acid with **29** in 81% yield. Palladium-catalyzed Sonogoshira coupling of **30** with aryl and cyclic alkyl acetylenes provided the desired western analogues **31** in 50−90% yield. When the desired acetylene coupling partners were unavailable, analogues were synthesized from terminal acetylene **33**. Sonogoshira coupling of 5-bromo-picolinamide **30** with trimethylsilylacetylene to yield **32**, followed by removal of the silyl protecting group with K_2CO_3 in MeOH/THF, provided terminal acetylene **33** in 73% yield over 2 steps. Sonogoshira coupling of the resulting terminal acetylene with aryl and heteroaryl bromides provided the desired analogues in 43−62% yield.

Synthesis of heteroaryl core analogues was achieved as displayed in Scheme 3. Sonogoshira coupling of 4-bromo-heteroaryl carboxylic acids **34a** and 1-ethynyl-3-fluorobenzene yielded biaryl acetylenes **35a** in 30−97% yield, which were then subjected to a HATU-mediated amide bond coupling with **29** to access core analogues **36**. Where the desired carboxylic acids were not available, the corresponding esters **34b** were used to access intermediate **34b** via a Sonogoshira coupling with 1-ethynyl-3-fluorobenzene. Saponification of ester **35b** with LiOH in THF/H_2O and amide coupling with **29** yielded the desired analogues.

The eastern amide region was explored utilizing ethynyl-picolinic acid **37** as shown in Scheme 4. Following coupling of 5-bromopicolinic acid with 1-ethynyl-3-fluorobenzene to yield **37**, a variety of amines were installed through HATU-mediated amide bond formation. To understand the effect of the chiral center, (*S*)-3-amino-2-methylbutan-2-ol was prepared from L-alanine in a sequence analogous to that shown in Scheme 1, and a variety of commercially available chiral amines bearing the (*R*)- and (*S*)-configuration at the chiral center were investigated. In addition, to systematically explore the effects of the eastern hydroxyl on ago-PAM activity, several additional analogues were prepared directly from **19**. Methylation of the tertiary hydroxyl by treatment with NaH in THF followed by reaction with MeI afforded methyl ether **38f**. The hydroxyl group was also transformed into the corresponding fluoro-analogue via reaction of the alcohol with DAST (CH_2Cl_2, −78 °C) to access **38e**.

In Vitro Pharmacology. Compounds were profiled in our rat $mGlu_5$ low receptor expression cell line using a "triple add" protocol in accord with previously published procedures.[42,43] Activity observed using the low receptor expressing cell line correlates with the functional response observed in native systems and allows for detection of allosteric agonism. The "triple add" protocol allows compounds to be evaluated for agonism as well as positive and negative allosteric modulation simulataneously.[43]

The structure−activity relationship (SAR) are shown in Tables 1−3. SAR around the western aryl region reveals that most manipulations to this portion of the molecule do not eliminate ago-PAM activity. As seen in compounds **19**, **31b**, and **31c**, positioning of the fluorine atom only modestly affected potency and efficacy with des-fluoro compound **31a** and 3-fluoro congener **19** preferred for both agonist and PAM potency. Incorporation of the sterically larger methyl group led to a concomitant decrease of PAM and agonist activity, except in the case of *meta*-substituted analogue **31g**. While agonism was retained for *ortho*- and *meta*-substituted derivatives **31f** and **31g**, methyl substitution at the *para*-position led to PAM **31h**. Introduction of a western pyridyl also proved to impact agonist activity, leading to the discovery of PAM **31i**, bearing a western 2-pyridine. Structurally, **31i** is intriguing as PAM to NAM mode switching has been observed upon the introduction of the 2-pyridyl functionality within the tetralone acetylene series reported by Merz Pharmaceuticals[29] and in the acetylene scaffold reported by Ritzén and co-workers (Figure 6).[31,44] Thus, it appears that, within the acetylene scaffold, the 2-pyridyl functionality can engender inhibitory effects in some cases. Moreover, when functionalities are present in other regions of the molecule that lead to receptor activation (e.g., agonism or ago-PAM), the 2-pyridyl group appears to moderate these strong agonist effects. The positioning of the pyridyl nitrogen also appears to be critical for attenuation of the agonism, as the 3- and 4-substituted pyridines (**31j**, **31k**) maintain ago-PAM activity. Given that the 2-pyridiyl motif is structurally reminiscent of $mGlu_5$ antagonist MPEP, we also investigated the methyl thiazole motif found in the $mGlu_5$ antagonist MTEP to give **31l**, which also elicited a PAM profile with no observed agonism. Finally, cyclic alkyl groups were explored, with cyclopropyl derivative **31m** found to be a PAM, although with greatly reduced potency. Ago-PAM cyclopentyl derivative **31n** exhibited a smaller degree of allosteric agonism relative to aryl analogues.

Table 1. Rat $mGlu_5$ Potency and Percent GluMax Response for Western Aryl Analogues

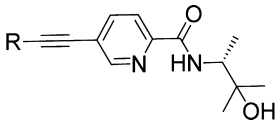

		Potentiator (Rat $mGlu_5$)			Agonist (Rat $mGlu_5$)			
Compound	**R**	**pEC_{50} (± SEM)[a]**	**EC_{50} (nM)[a]**	**GluMax (± SEM)[a]**	**pEC_{50} (± SEM)[a]**	**EC_{50} (nM)[a]**	**GluMax (± SEM)[a]**	**Category**
31a		8.38 ± 0.14	4.1	60.9 ± 5.1	6.06 ± 0.14	874	43.2 ± 5.2	ago-PAM
31b		8.10 ± 0.07	8.0	60.0 ± 2.9	5.94 ± 0.10	1,160	29.6 ± 4.0	ago-PAM
19	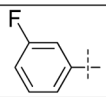	8.31 ± 0.02	4.9	63.5 ± 2.7	6.04 ± 0.10	904	37.1 ± 5.7	ago-PAM
31c	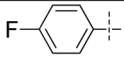	7.91 ± 0.07	12.3	66.2 ± 2.1	5.82 ± 0.12	1,520	38.4 ± 5.7	ago-PAM
31d	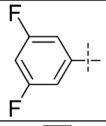	7.24 ± 0.10	58.2	61.6 ± 1.4	5.44 ± 0.01	3,670	37.9 ± 4.3	ago-PAM
31e	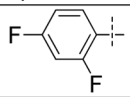	7.58 ± 0.09	26.6	61.2 ± 1.4	5.43 ± 0.18	3,690	38.2 ± 8.9	ago-PAM
31f		6.66 ± 0.04	217	59.9 ± 1.8	4.91 ± 0.02	12,400	24.1 ± 5.3	ago-PAM
31g		8.19 ± 0.16	6.5	68.6 ± 3.3	5.87 ± 0.03	1,360	20.8 ± 2.9	ago-PAM
31h		6.97 ± 0.02	107	63.1 ± 2.0	--	--	--	**PAM**
31i		7.38 ± 0.19	41.3	57.5 ± 6.14	--	--	--	**PAM**
31j		6.46 ± 0.03	344	71.5 ± 4.4	5.03 ± 0.05	9,300	25.9 ± 8.3	ago-PAM
31k	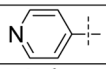	7.37 ± 0.13	43.0	66.6 ± 2.6	5.33 ± 0.06	4,660	22.4 ± 6.6	ago-PAM
31l	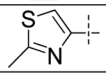	7.23 ± 0.50	58.4	66.6 ± 3.0		--	--	**PAM**
31m		5.89 ± 0.00	1289	63.4 ± 6.0	--	--	--	**PAM**
31n		7.03 ± 0.28	93.3	63.7 ± 3.8	5.01 ± 0.06	9,750	14.8 ± 5.7	ago-PAM

[a] pEC_{50}, EC_{50}, and % GluMax response are the average of at least three independent measurements performed in duplicate or triplicate.

In parallel, explorations of the core region of the molecule revealed interesting structural features of allosteric agonism. Deletion of the nitrogen in benzamide **36a** yielded a highly potent ago-PAM (Table 2). Interestingly, although nicotinamide analogue **36b** displayed reduced potency in comparison with picolinamide **19**, it still displayed significant allosteric agonism. As nicotinamide acetylene analogues exemplified by **20** (Figure 3) and **26** (Figure 5) are generally PAMs devoid of agonsim, these results suggest that the eastern amide portion of the molecule is partially responsible for the observed allosteric agonism. Core modifications were able to eliminate allosteric agonism in some instances, as 3- and 4-substituted methyl analogues **36d** and **36e** as well as pyrimidine **36f** were found to lack apparent agonist activity. Regioisomeric pyrimidine **36g**, however, displayed ago-PAM activity, as did pyridazine, pyrazine, and thiazole core analogues (**36h**−**36j**).

We next turned our attention to exploring the eastern amide region within the picolinamide core as this structural motif appeared to have a significant bias toward ago-PAM activity. Maintaining the propyl backbone found in **19**, we prepared a number of analogues, systematically varying substituents to explore the SAR profile of allosteric agonism (Table 3). On the

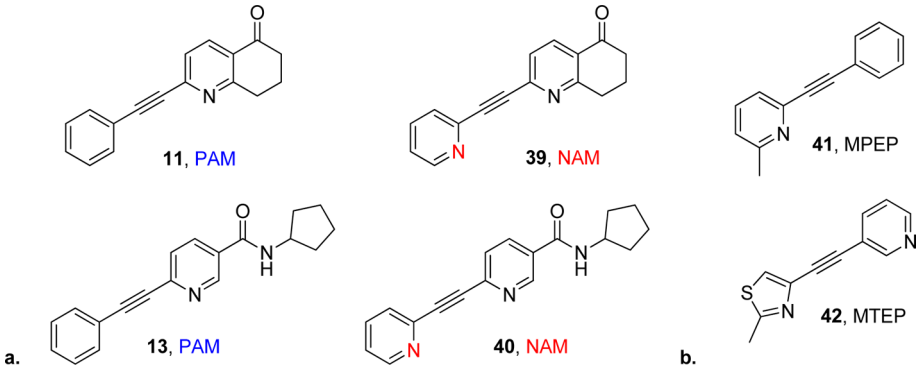

Figure 6. (a) PAM to NAM mode switching with incorporation of the 2-pyridyl motif.[29,44] (b) Acetylene-based allosteric antagonists.

Table 2. Rat mGlu$_5$ Potency and Percent GluMax Response for Core Analogues

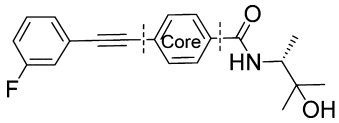

		Potentiator (Rat mGlu$_5$)			Agonist (Rat mGlu$_5$)			
Compound	**R**	**pEC$_{50}$ (± SEM)** [a]	**EC$_{50}$ (nM)** [a]	**GluMax (± SEM)** [a]	**pEC$_{50}$ (± SEM)** [a]	**EC$_{50}$ (nM)** [a]	**GluMax (± SEM)** [a]	**Category**
36a	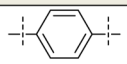	8.12 ± 0.06	7.5	53.9 ± 4.3	5.98 ± 0.03	1,040	43.6 ± 4.3	ago-PAM
19	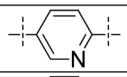	8.31 ± 0.02	4.9	63.5 ± 2.7	6.04 ± 0.10	904	37.1 ± 5.7	ago-PAM
36b	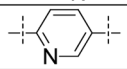	7.10 ± 0.04	80.0	64.9 ±1.5	5.17 ± 0.08	6,800	26.6 ± 5.1	ago-PAM
36c	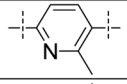	7.77 ± 0.05	17.1	64.9 ± 2.1	5.96 ± 0.01	1,090	9.2 ± 1.7	ago-PAM
36d	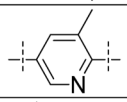	6.98 ± 0.04	105.4	66.4 ± 3.2	--	--	--	**PAM**
36e	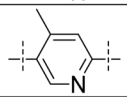	6.62 ± 0.04	242.1	66.6 ± 1.2	--	--	--	**PAM**
36f	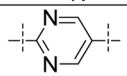	6.91 ± 0.13	121.8	68.7 ± 3.1	--	--	--	**PAM**
36g	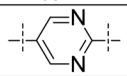	7.32 ± 0.18	47.6	64.1 ± 3.0	5.38 ± 0.22	4,130	19.2 ± 5.5	ago-PAM
36h	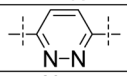	7.66 ± 0.07	21.9	70.2 ± 3.4	5.67 ± 0.05	2,120	16.5 ± 3.9	ago-PAM
36i	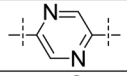	7.90 ± 0.03	12.5	64.4 ± 3.1	5.52 ± 0.02	3,040	17.2 ± 3.7	ago-PAM
36j	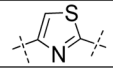	7.48 ± 0.05	33.5	62.1 ± 3.8	5.32 ± 0.03	4,780	26.1 ± 2.9	ago-PAM

[a] pEC$_{50}$, EC$_{50}$, and % GluMax response are the average of at least three independent measurements performed in duplicate or triplicate.

basis of our initial hypothesis that the tertiary carbinol contributes to allosteric agonism and adverse effects, our first round of SAR involved deletion and modification of the tertiary hydroxyl. Surprisingly, *tert*-butyl analogues **38a** and **38b** and isopropyl analogues **38c** and **38d** displayed potent ago-PAM activity, and replacement of the hydroxyl with fluorine (**38e**) resulted in a potent ago-PAM.

For optically active compounds **38a**−**38d** a slight preference was observed for the (*R*)-enantiomer. Interestingly, capping the tertiary carbinol as the methyl ether (**38f**) resulted in an inactive compound. As changes to the tertiary carbinol were not

Table 3. Rat mGlu$_5$ Potency and Percent GluMax Response for Eastern Amide Analogues Lacking Polar Functionalities

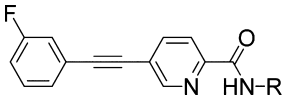

		Potentiator (Rat mGlu$_5$)			Agonist (Rat mGlu$_5$)			
Compound	R	pEC$_{50}$ (± SEM)[a]	EC$_{50}$ (nM)[a]	GluMax (± SEM)[a]	pEC$_{50}$ (± SEM)[a]	EC$_{50}$ (nM)[a]	GluMax (± SEM)[a]	Category
38a		7.75 ± 0.19	17.8	66.0 ± 2.7	5.56 ± 0.07	2,751.8	31.2 ± 2.7	ago-PAM
38b		7.28 ± 0.12	51.9	70.8 ± 3.6	5.27 ± 0.17	5,403.4	20.0 ± 2.8	ago-PAM
38c		8.35 ± 0.09	4.5	69.3 ± 0.8	5.83 ± 0.25	1,469.1	22.5 ± 1.4	ago-PAM
38d		7.69 ± 0.11	20.4	66.7 ± 2.7	5.65 ± 0.04	2,224.1	13.1 ± 1.4	ago-PAM
38e		8.28 ± 0.04	5.3	68.6 ± 3.0	5.69 ± 0.08	2,064.5	42.8 ± 2.5	ago-PAM
38f	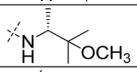	--	--	--	--	--	--	Inactive
38g		7.46 ± 0.04	34.4	65.9 ± 1.3	5.52 ± 0.03	3,009.9	8.3 ± 2.2	ago-PAM
38h		7.54 ± 0.03	28.9	58.2 ± 2.7	--	--	--	**PAM**
38i		7.78 ± 0.13	16.6	63.9 ± 1.0	5.59 ± 0.25	2,573.1	9.5 ± 2.1	ago-PAM
38j		7.43 ± 0.10	36.7	61.4 ± 1.6	--	--	--	**PAM**
38k	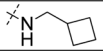	7.08 ± 0.12	84.0	68.1 ± 3.44	< 5.0	> 10,0000.0	4.7 ± 1.3	ago-PAM

[a]pEC$_{50}$, EC$_{50}$, and % GluMax response are the average of at least three independent measurements performed in duplicate or triplicate.

successful in preventing ago-PAM activity, we deleted the methyl group adjacent to the amide while maintaining the eastern alkyl chain carbon backbone length found in **19**. This exploration proved fruitful with isobutyl analogue **38h** and methyl-cyclopropyl analogue **38j** found to be potent PAMs; however, the effect was subtle and the trend was not entirely clear as the propyl analogue **38g**, *tert*-butyl analogue **38i**, and methyl-cyclobutyl analogue **38k** displayed weak agonism.

Since deletion of the tertiary carbinol did not yield a general strategy to prevent allosteric agonism, we next explored analogues bearing the eastern alcohol in order to gain an understanding of the SAR of allosteric agonism when a hydrogen bond donor was maintained (Table 4). The effect of the configuration of the stereogenic center was first explored, and surprisingly, the opposite enantiomer of **19**, (*S*)-**38l**, was inactive, suggesting that the position of the tertiary hydroxyl group is critical in receptor activation at the allosteric binding site. In contrast, both enantiomers of optically active derivatives **38a**–**38d** were active ago-PAMs, with only a slight preference for the (*R*)-enantiomer. Removal of steric bulk surrounding the alcohol (**38m**) and adjacent to the amide (**38n**) did not remove allosteric agonism, while alcohol **38o** possessing no steric bulk was inactive. Interestingly, extension of the carbon backbone in analogue **38p** resulted in a loss of agonist activity, suggesting that allosteric agonism within this series is sensitive to the location of the tertiary carbinol.

We next pursued alternatives to the tertiary carbinol, investigating functional groups that conceptually could serve as a "molecular lock", such that the functionality possesses desirable physiochemical and DMPK properties, which intentionally deter formation of hydroxylated metabolites specifically within the eastern amide moiety that may engender undesirable pharmacology on their own.[38] Fluorinated alkyl amides were explored, and trifluoroethyl derivative **38q** was found to be an ago-PAM with moderate potency. Trifluoroalkyl derivatives possessing a chiral center afforded increased activity (**38r**–**38s**). Interestingly, these analogues yielded enantiospecific activity, with (*R*)-**38r** representing a highly potent PAM and (*S*)-**38s** displaying ago-PAM activity. We also explored oxetanes since this motif has been utilized as a surrogate for geminal dimethyl groups and represent a polar alternative for the introduction of steric bulk as well as possessing hydrogen bond accepting properties.[45] In particular, the oxetane was appealing as a means to address the high lipophilicity and plasma protein binding associated with our recently reported PAM VU0405386 (**43**);[46] thus, we prepared the 3-methyl-substituted oxetane as a *tert*-butyl replacement (**38t**, Figure 7). The oxetane can also be envisioned as an isosteric replacement for the cyclobutyl moiety found in **21** (Figure 3), which was found to generate the 3-hydroxy metabolite **22** (Figure 3) that contributed in part to an adverse effect profile. Incorporation of the oxetane moiety proved successful and **38t** represents the most potent PAM (EC$_{50}$ = 9.3 nM) discovered thus far within this series. Maintaining the oxetane and extending the carbon chain length one carbon led to equipotent PAM **38u**. Further extension to the two-carbon variant **39v** maintained potentiation activity; however, weak allosteric agonism returned (EC$_{50}$ = 2.8 μM, GluMax 16.3%). Collectively, the eastern amide SAR

Table 4. Rat mGlu$_5$ Potency and Percent GluMax Response for Eastern Amide Analogues Bearing Polar Functionalities

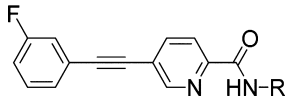

		Potentiator (Rat mGlu$_5$)			Agonist (Rat mGlu$_5$)			
Compound	R	pEC$_{50}$ (± SEM)[a]	EC$_{50}$ (nM)[a]	GluMax (± SEM)[a]	pEC$_{50}$ (± SEM)[a]	EC$_{50}$ (nM)[a]	GluMax (± SEM)[a]	Category
19	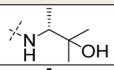	8.31 ± 0.02	4.9	63.5 ± 2.7	6.04 ± 0.10	904	37.1 ± 5.7	ago-PAM
38l	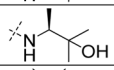	--	--	--	--	--	--	Inactive
38m	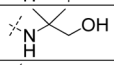	8.10 ± 0.11	7.9	60.9 ± 4.6	6.14 ± 0.10	729	9.3 ± 3.3	ago-PAM
38n	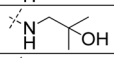	7.46 ± 0.02	34.6	61.5 ± 2.5	5.40 ± 0.08	4,020	20.0 ± 6.0	ago-PAM
38o	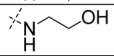	--	--	--	--	--	--	Inactive
38p	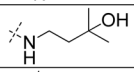	6.87 ± 0.04	136	61.9 ± 2.8	--	--	--	**PAM**
38q		6.65 ± 0.09	224	67.0 ± 1.7	4.97 ± 0.22	10,700	5.8 ± 1.1	ago-PAM
38r		7.68 ± 0.11	20.8	52.1 ± 7.1	--	--	--	**PAM**
38s		7.66 ± 0.03	21.9	60.8 ± 4.7	5.86 ± 0.01	1,390	21.4 ± 2.2	ago-PAM
38t		8.03 ± 0.06	9.3	45.5 ± 2.4	--	--	--	**PAM**
38u	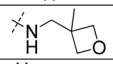	7.97 ± 0.23	10.7	60.4 ± 3.4	--	--	--	**PAM**
38v	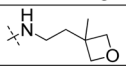	7.33 ± 0.11	47.3	65.7 ± 5.0	5.55 ± 0.03	2,840	16.3 ± 2.5	ago-PAM

[a]pEC$_{50}$, EC$_{50}$, and % GluMax response are the average of at least three independent measurements performed in duplicate or triplicate.

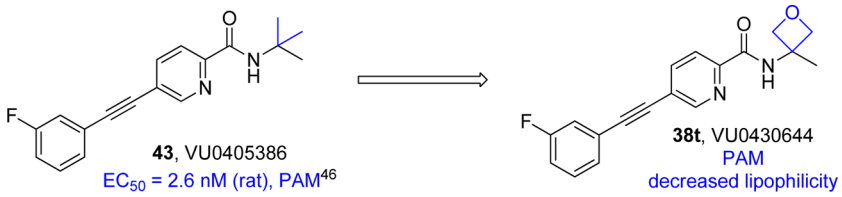

Figure 7. Oxetane surrogate for steric bulk with decreased lipophilicity.

strongly suggests that the general structural elements of the 2-methylbutan-2-ol motif (**29**) introduced to increase solubility are strongly biased toward allosteric agonism and that other eastern amide groups can be identified with favorable physiochemical properties that result in PAMs lacking agonist activity.

In light of these results, a final round of SAR was pursued to probe the effects of the basicity of the pyridyl nitrogen in pure PAM **31i** and to investigate combination of the western pyridyl with a small subset of eastern alkyl groups such as the oxetane motif. We first studied the effects of the basicity of the pyridyl nitrogen through the introduction of electron-withdrawing fluorine atoms around the pyridine ring. If a basic nitrogen at the 2-position of the pyridine ring helps to stabilize a conformation of the receptor not disposed toward allosteric agonism, we hypothesized that decreased basicity of the pyridyl nitrogen at this position might weaken this interaction and restore allosteric agonism. As shown in Table 5, introduction of fluorine reveals that the basicity of the pyridyl nitrogen is in fact important, as fluoro-substituted pyridyls **31o**−**31r** display allosteric agonism. We subsequently designed several analogues to explore whether the 2-pyridyl functionality could serve as a "molecular lock" to prevent allosteric agonism in compounds bearing eastern amide alkyl groups found to possess agonism when combined with the 3-fluorophenyl western aryl ring. This study revealed that the 2-pyridyl motif prevented allosteric agonism in some but not all cases. Modulator **44b** and **44c** exhibited PAM activity; however, *tert*-butyl analogue **44a** displayed ago-PAM activity. We then pursued a hybrid picolinamide acetylene containing the western 2-pyridyl and eastern oxetane amide motifs since these substructures were discovered to be two of the most preferred structural elements to maintain PAM activity without apparent agonism (**44d**). Unexpectedly, this combination led to mode switching, yielding

Table 5. Rat $mGlu_5$ Potency and Percent GluMax Response for Pyridyl Analogues

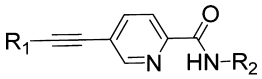

			Potentiator (Rat $mGlu_5$)			Agonist (Rat $mGlu_5$)			
Compd	**R_1**	**R_1**	**pEC_{50} (± SEM)[a]**	**EC_{50} (nM)[a]**	**GluMax (± SEM)[a]**	**pEC_{50} (± SEM)[a]**	**EC_{50} (nM)[a]**	**GluMax (± SEM)[a]**	**Category**
31i	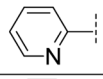	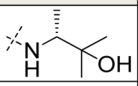	7.03 ± 0.14	92.9	69.7 ± 4.3	--	--	--	**PAM**
31o	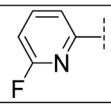	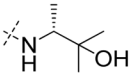	7.87 ± 0.24	13.6	63.0 ± 1.7	5.89 ± 0.15	1,300	8.3 ± 2.4	ago-PAM
31p	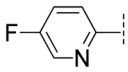	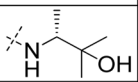	7.55 ± 0.07	28.2	64.6 ± 3.0	5.77 ± 0.04	1,700	13.5 ± 3.1	ago-PAM
31q	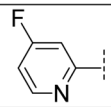	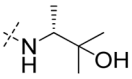	7.44 ± 0.36	36.0	66.2 ± 2.8	5.40 ± 0.22	3,980	33.0 ± 7.8	ago-PAM
31r	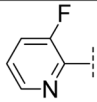	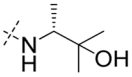	7.47 ± 0.04	33.8	60.6 ± 4.3	5.43 ± 0.01	3,700	29.2 ± 3.6	ago-PAM
44a	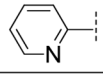	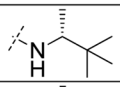	7.20 ± 0.06	63.3	63.0 ± 4.9	5.21 ± 0.06	6,110	24.2 ± 3.7	ago-PAM
44b		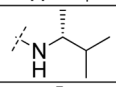	7.10 ± 0.07	79.0	58.5 ± 3.0	--	--	--	**PAM**
44c		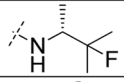	7.65 ± 0.10	22.2	54.9 ± 3.3	--	--	--	**PAM**
44d		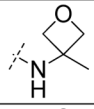	6.14 ± 0.20[b]	731[b]	16.7 ± 4.5[b]	--	--	--	antagonist
45	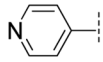	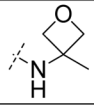	6.16 ± 0.10	691	36.0 ± 6.9		--	--	Weak PAM

[a] pEC_{50}, EC_{50}, and % GluMax response are the average of at least three independent measurements performed in duplicate or triplicate. [b] pIC_{50}, IC_{50}, and GluMin are the average of three independent measurements performed in triplicate.

an antagonist. Moving the nitrogen to the 4-position and maintaining the oxetane (**45**) restored some potentiation, resulting in a weak PAM.

In an effort to gain further insights into the interaction of ago-PAM versus PAM preferring functional groups within the $mGlu_5$ binding pocket, PAMs **31i** and **38t** along with ago-PAM **19** were docked into our recently generated comparative model of the transmembrane region of $mGlu_5$ (Figure 8).[47] Interestingly, in comparison with previously docked picolinamide PAMs (e.g., **43** and **21**),[47] all three compounds sit higher in the binding pocket; this may be attributable to the inclusion of the additional hydrogen bond acceptor on the eastern amide. Similar to what we observed for other acetylenic PAMs, computationally it was difficult to differentiate whether the eastern amide is buried deep within the pocket, or points toward the extracellular space, likely a reflection of the highly linear structure for the class. However, models wherein the eastern amide points toward the extracellular space placed the compounds in proximity of residues previously found to be critical for the function of acetylene PAMs and MPEP (Figure 8).[47] The hydroxyl and amide carbonyl of the modulators were within 3 Å of S808, and the 2-pyridyl western aryl ring was within 3−5 Å from Y658, T780, and W784. This pose was chosen as the most likely binding conformation due to its

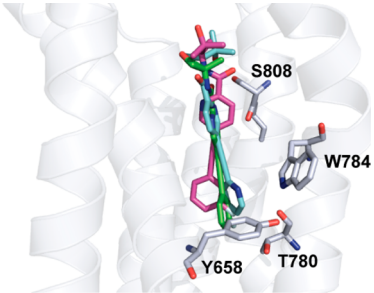

Figure 8. $mGlu_5$ binding pose for pure-PAMs **31i** (cyan color) and **38t** (green color) and ago-PAM **19** (magenta).

Table 6. Rat $mGlu_5$ Cooperativity (Fold-Shift) of Selected PAMs Lacking Apparent Allosteric Agonist Activity

Compound	Structure	Glumate Fold-Shift	Compound	Structure	Glutamate Fold-Shift
31i	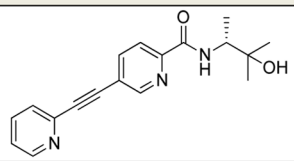	1.7	**38p**	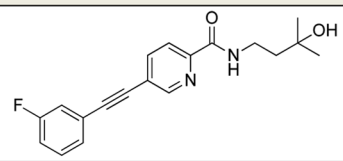	5.3
31l	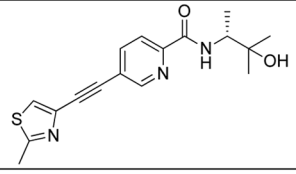	1.6	**38r**	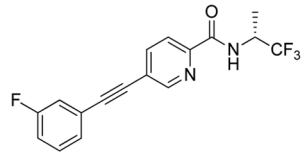	1.5
36d	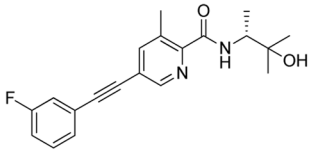	2.3	**38t**	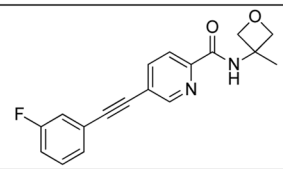	2.8
36f	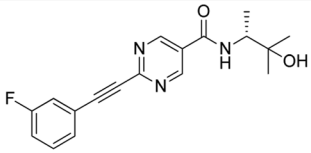	4.0	**38u**	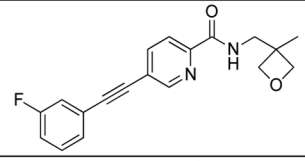	3.3
38h	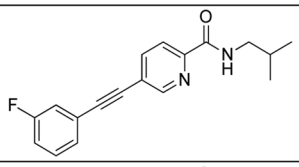	1.9	**44b**	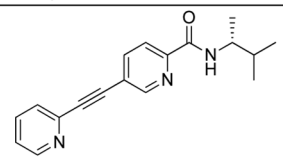	1.3
38j	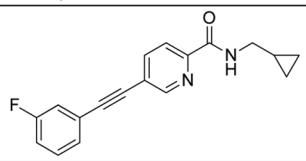	1.6	**44c**	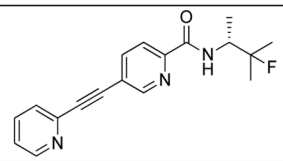	1.5

[a]PAM concentration tested was 10 μM. Values represent the average of three independent measurements performed in triplicate.

consistency with existing data, and the second possible pose is shown in the Supporting Information (see section VI).

In an attempt to probe these putative poses and elucidate the molecular determinants of agonism further, we examined the impact of four key point mutations (Y658V, T780A, W784A and S808A) on modulator affinity, cooperativity, and agonism by applying an operational model of allosterism to glutamate concentration−response curves in the absence and presence of varying concentrations of each PAM, i.e., a progressive fold-shift experiment (Supporting Information, see sections II−V). All three compounds were sensitive to alanine substitution of T780A; however, the observed reductions in affinity (10−30-fold) were not as substantial as those reported for previous picolinamides (e.g., **43** and **21**).[47] The overall profile of **38t** across all four point mutations was comparable to the prior picolinamides,[47] and in particular both Y658V and S808A engendered a NAM switch identical to previously reported (5-((3-fluorophenyl)ethynyl)pyridin-2-yl)(3-hydroxyazetidin-1-yl)methanone (VU0405398).[47] The most striking differences are observed for **31i**, as Y658V had no effect on affinity or cooperativity, despite causing marked reductions in affinity, including abolishment of PAM activity, for all other picolinamide PAMs tested to date. Furthermore, **31i** showed a gain in allosteric agonist activity at W784A, a mutation known to reduce the negative cooperativity of MPEP and increase positive cooperativity of other PAMs.[47] On the basis of the pose depicted in Figure 8 and the 2-pyridyl "molecular switch" trends discussed previously (vide supra, see Figure 6), it may be hypothesized that the 2-pyridyl western aryl within acetylenic $mGlu_5$ modulators has a key interaction with W784, favoring less active receptor states. In the W784A mutant where this interaction is absent, modulator **31i** more readily facilitates active receptor conformations.

Having gained insights into the allosteric agonism SAR and potential models for receptor/residue-ligand interaction, we turned our attention to PAM glutamate cooperativity due to its impact on therapeutic index. We selected PAMs lacking agonist activity from this investigation that display potency values ≤200 nM and evaluated their ability to left shift the glutamate concentration−response curve at a concentration of 10 μM (Table 6). This analysis revealed a range of glutamate fold-shift values from 1.3 to 5.3. This distribution of fold-shift values provides useful tool compounds to probe the impact of cooperativity on therapeutic index in PAMs within the biaryl acetylene chemotype. As a result of its excellent potency and

low cooperativity, PAM **38t** was selected for further characterization and declared an MLPCN probe.

To validate that **38t** interacts with $mGlu_5$ at the MPEP binding site, radioligand binding studies were performed with [^{3}H]methoxyPEPy. Increasing concentrations of **38t** resulted in complete inhibition of [^{3}H]methoxyPEPy binding, supporting a competitive interaction between the two ligands (Figure 9). **38t**

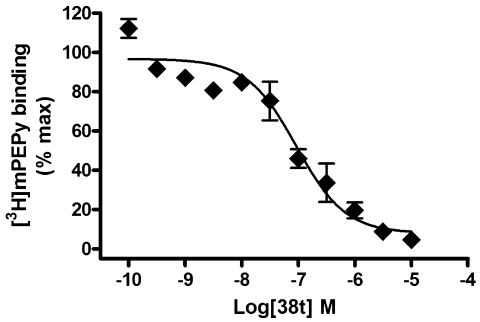

Figure 9. Compound **38t** fully displaces [^{3}H]methoxyPEPy binding.

exhibited a K_i of 90 nM, representing a ~10-fold higher functional activity (EC_{50} = 9.3 nM) compared to binding. To utilize compounds in in vivo assays it is important to determine if they are selective for $mGlu_5$ compared with other mGlu subtypes. A 10 μM concentration of PAM **38t** did not shift the glutamate (or L-AP4) concentration−response curve when evaluated using cells expressing any of the other mGlu subtypes ($mGlu_{1-4,6-8}$, see Supporting Information section I) demonstrating high selectivity for $mGlu_5$. In addition, screening of 10 μM **38t** against a panel of 68 GPCRs, ion channels, and transporters revealed no significant off-target activity (Eurofins Inc.). Finally, oxetane **38t** was evaluated in progressive fold-shift experiments (50 nM to 30 μM). The shift in the glutamate concentration−response curve in the presence of increasing concentrations of modulator is shown in Figure 10. Increasing

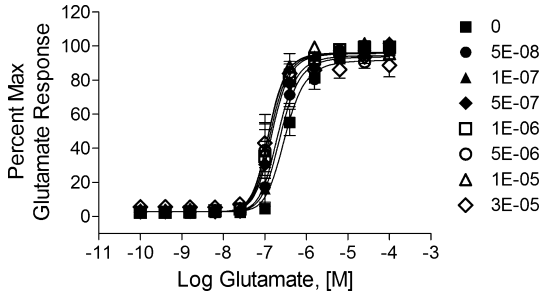

Figure 10. Compound **38t** shifts the glutamate concentration−response curve leftward with increasing concentrations of modulator: 1.7 at 50 nM; 1.7 at 100 nM; 2.2 at 500 nM; 2.7 at 1 μM; 3.0 at 5 μM; 2.8 at 10 μM and 3.2 at 30 μM.

concentration of modulator resulted in a fold-shift that reached a maximum of approximately 3.0-fold at 5 μM with a predicted affinity of −6.81 (154 nM) and an efficacy cooperativity factor (log β) between glutamate and indicated allosteric modulator of 0.34 (cooperativity ~2.2).

The in vitro drug metabolism and pharmacokinetic (DMPK) profile of **38t** was next determined, with the hope that the oxetane motif would help to mitigate previously observed metabolism and improve physiochemical properties within this chemotype. Gratifyingly, oxetane **38t** displayed low in vitro metabolism with a predicted hepatic clearance (CL_{HEP}) of 1.6 mL/min/kg in rat and 0.2 mL/min/kg in human, a significant improvement in comparison to similar compounds within this series (**19**, predicted CL_{HEP} of 34.5 mL/min/kg in rat and 3.5 mL/min/kg in human; **21**, predicted CL_{HEP} of 55.6 mL/min/kg in rat[38]). PAM **38t** also possesses improved fraction unbound (f_u) as measured by plasma protein binding assay using equilibrium dialysis, with oxetane **38t** 3.5% unbound in human plasma and 3.6% unbound in rat plasma. In comparison, more lipophilic **21** displays human and rat f_u plasma values <1%.[38] Rat brain homogenate binding was used to determine fraction unbound in brain for **38t**; these studies revealed f_u brain values of 1.6%. To assess drug−drug interactions, inhibition of the major human cytochrome P450 (CYP) enzymes (2C9, 2D6, 3A4, 1A2) was measured in human liver microsomes, and **38t** was found to display inhibitory activity at 1A2 (IC_{50} = 5.30 μM), while no activity was observed against the other CYPs tested (IC_{50} >30 μM). Solubility of **38t** was found to be modest with a Fassif (fasted simulated intestinal fluid) solubility of 10−23 μg/mL.

To verify its PAM pharmacological profile in native systems, **38t** was examined for induction of long-term depression (LTD) at the Schaffer collateral-CA1 (SC-CA1) synapse in the hippocampal formation. LTD at this synapse is known to be modulated by $mGlu_5$ activation, and orthosteric $mGlu_5$ agonists such as (*S*)-3,5-DHPG have been shown to elicit LTD.[48] Similarly ago-PAM **19** induces LTD;[38] however, **38t** does not induce LTD on its own (Figure 11; 100.3 ± 3.7% baseline 55

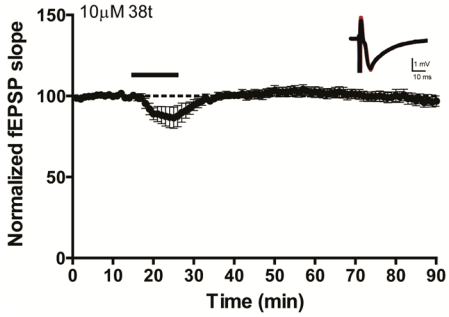

Figure 11. Compound **38t** has no effect on long-term depression at the SC-CA1 synapse in rat hippocampus.

min after compound washout). This provides further evidence that **38t** does not elicit a response on its own in native systems. In addition, prior studies involving **19** showed the induction of epileptiform activity in CA3 pyramidal neurons in hippocampal preparations. We performed similar studies with **38t** to assess agonist activity in this native CNS preparation. PAM **38t** had no significant effect on either the interevent interval (127.9 ± 7.7% of baseline) or amplitude (101.2 ± 5.0% of baseline) of spontaneous firing supporting an agonism-free profile for **38t** (data not shown). These data demonstrate that **38t** acts as a pure PAM in two hippocampal native systems.

■ CONCLUSION

Although $mGlu_5$ PAMs represent a promising therapeutic strategy for the treatment of schizophrenia, recent reports have raised concerns over a seizure liability and neurotoxicity associated with some chemotypes. Allosteric agonism within the **19** acetylene chemotype and a high cooperativity (glutamate fold-shift) within the Merck-Addex piperidine and

caprolactam series are pharmacological profiles that have been associated with an adverse effect liability. We have extensively explored the SAR of allosteric agonism within the acetylene amide chemotype, providing insight into the structural elements contributing to allosteric agonism. In general, the structural elements of the eastern amide were found to have the greatest impact on the presence or absence of allosteric agonism. Replacement of the western 3-fluorophenyl with the 2-pyridyl motif was found to eliminate allosteric agonism in many but not all cases. The computational docking and mutagenesis data highlight the subtleties of interactions within the common allosteric site, wherein key residues, in particular W784 and S808, are hypothesized to be engaged in key interactions important for receptor−modulator interaction and function. Future studies to understand if the functional consequences of these mutants are indicative of a direct residue side chain−modulator interaction or an indirect allosteric interaction will be important to pursue.

Because of the potential impact of cooperativity on adverse effects, the glutamate fold-shift profile of potent PAMs was examined, revealing PAMs possessing low to moderate efficacy as assessed by glutamate fold-shift. This distribution of cooperativity profiles will enable studies to test the impact of glutamate fold-shift on neurotoxicity within this chemotype. On the basis of its efficacy profile and lack of apparent agonism in vitro, highly potent oxetane **38t** was further characterized and found to possess significantly improved DMPK properties compared with other acetylenes within this series. **38t** was also profiled in native systems and exhibited no allosteric agonism for the induction of LTD at the Schaffer collateral-CA1 (SC-CA1) synapse or epileptiform activity in CA3 pyramidal neurons. Preliminary experiments using a high dose of **38t** in an in vivo model of psychosis demonstrate robust reversal of amphetamine-induced hyperlocomotion (data not shown) with no overt behavioral disturbances; however, definitive PK-PD studies in this and other models, including fluorojade neurotoxicity studies, are needed in order to fully ascertain the anticipated in vivo properties of PAM **38t**. PAM **38t** represents a highly potent tool compound with acceptable pharmacokinetic properties that will enable further studies to probe the therapeutic index of low fold-shift PAMs. Such studies involving **38t** and other structurally diverse PAMs are underway and will be reported in due course. $mGlu_5$ PAM **38t** (ML254) is an MLPCN probe and is freely available upon request.[60]

■ EXPERIMENTAL SECTION

General. All reagents purchased from commercial suppliers were used without purification. Unless noted all solvents used were anhydrous and all reactions were carried out under argon atmosphere. Analytical thin layer chromatography was performed on Analtech silica gel GF 250 μm plates. Preparative RP-HPLC purification was performed on a Gilson Inc. preparative UV-based system using a Phenomenex Luna C18 column (50 mm × 30 mm i.d., 5 μm) with an acetonitrile (unmodified)/0.1% trifluoroacetic acid in water gradient. Normal-phase silica gel preparative purification was performed using an automated Combi-flash Rf from ISCO. Analytical LC−MS was performed on an Agilent 1200 Series with UV detection at 215 and 254 nm and ELSD detection (Polymer Laboratories PL-ELS 2100), utilizing an Accucore C18 2.6 μm, 2.1 mm × 30 mm column, a 1.1 min gradient, 7% [CH_3CN/0.1% TFA] to 95% [CH_3CN/0.1% TFA], and a G6130 single quadrupole mass spectrometer. Purity of all final compounds was determined to be >98% by analytical HPLC. Solvents for extraction, washing, and chromatography were HPLC grade. NMR spectra were recorded on a Bruker 400 MHz spectrometer. ^{1}H chemical shifts are reported as δ values in $CDCl_3$ or $CDOD_3$. Data are reported as follows: chemical shift, integration, multiplicity (s = singlet, bs = broad singlet, d = doublet, t = triplet, q = quartet, p = pentet, hex = hextet, sep = septet, dd = doublet of doublets, dq = doublet of quartets, m = multiplet), coupling constant reported in Hz. ^{13}C chemical shifts are reported in δ values in $CDCl_3$ or $CDOD_3$ as follows: chemical shift, C−F coupling constants (J_{C-F}) reported in Hz. Low resolution mass spectra were obtained on an Agilent 1200 series 6130 mass spectrometer. HRMS were obtained using a Micromass (Waters) Q-Tof API-US calibrated and verified with sodium iodide. The samples were diluted with a 50:50 0.1% formic acid (in Milli-Q)/acetonitrile solution, directly infused using leucine-enkephalin (M + H = 556.2771) as a lockmass. Scan range was from 100 to 1000 Da, using a scan time of 1 s. The [M + H] or [M + Na] ion was observed. Optical rotation values were obtained on a JASCO P-2000 polarimeter.

Chemistry. (*R*)-*tert*-Butyl (3-Hydroxy-3-methylbutan-2-yl)-carbamate (28). D-Alanine (15 g, 0.168 mol, 1 equiv) was dissolved in MeOH (75 mL, 2.2 M) and cooled to 0 °C. $SOCl_2$ (20.8 mL, 0.286 mol, 1.7 equiv) was *slowly* added taking care to control the exotherm. The reaction mixture was stirred overnight warming to room temperature. After the reaction was determined to be complete by TLC, the MeOH and excess $SOCl_2$ were carefully removed by vacuum distillation. The resulting oil was redissolved in MeOH (50 mL), and the solvent was removed by rotary evaporation. The resulting methyl ester was dissolved in CH_2Cl_2 (150 mL, 1.1 M) and cooled to 0 °C. Et_3N (70.2 mL, 0.504 mol, 3 equiv) and Boc_2O (44 g, 0.202 mol, 1.2 equiv) were added, and the reaction mixture was allowed to warm to room temperature and stirred overnight. After the reaction was determined to be complete by TLC, the precipitates formed during the reaction were removed via filtration through Celite rinsing with CH_2Cl_2. The organic layer was washed with citric acid (satd aq, 1 × 50 mL), dried with Na_2SO_4, and concentrated via rotary evaporation yielding (*R*)-methyl 2-((*tert*-butoxycarbonyl)amino)propanoate as a yellow oil (30 g, 88% yield). $[\alpha]^{20}_D$ = 3.6 (*c* 1.3, $CHCl_3$); ^{1}H NMR (400 MHz, $CDCl_3$) δ 5.07 (1H, bs), 4.28 (1H, m), 3.71 (3H, s), 1.41 (9H, s), 1.35 (3H, d, *J* = 7.2 Hz); ^{13}C NMR (100 MHz, $CDCl_3$) δ 173.8, 155.0, 79.7, 52.2, 49.1, 28.2, 18.5; HRMS (ES+, M + H) calcd for $C_9H_{18}NO_4$ 204.1236, found 204.1236.

(*R*)-Methyl 2-((*tert*-butoxycarbonyl)amino)propanoate (5 g, 24.6 mmol, 1 equiv) was dissolved in THF (125 mL, 0.2 M) and cooled to 0 °C. MeMgBr (32.8 mL, 98.4 mmol, 5 equiv, 3.0 M soln in Et_2O) was added slowly, and the reaction was allowed to warm to room temperature and stirred overnight. The reaction was then quenched ***carefully*** with NH_4Cl (satd aq) and extracted with EtOAc (3 × 75 mL). The organic layer was dried with Na_2SO_4 and concentrated. The crude oil was purified by silica gel chromatography eluting with Hex/EtOAc (0−75% EtOAc) with the desired product eluting between 30% and 50% EtOAc. (*R*)-*tert*-Butyl (3-hydroxy-3-methylbutan-2-yl)carbamate was isolated as a clear oil (3.15 g, 63% yield). $[\alpha]^{20}_D$ = 1.9 (*c* 1.4, $CHCl_3$); ^{1}H NMR (400 MHz, $CDCl_3$) δ 4.82 (1H, d, *J* = 7.2 Hz), 3.54 (1H, bs), 2.58 (1H, bs), 1.41 (9H, s), 1.19 (3H, s), 1.14 (3H, s), 1.09 (3H, d, *J* = 6.8 Hz); ^{13}C NMR (100 MHz, $CDCl_3$) δ 156.3, 79.3, 72.8, 54.5, 28.3, 27.3, 25.6, 16.1; HRMS (ES+, M + H) calcd for $C_{10}H_{22}NO_3$ 204.1600, found 204.1598.

(*R*)-3-Amino-2-methylbutan-2-ol (29). In a scintillation vial, (*R*)-*tert*-butyl (3-hydroxy-3-methylbutan-2-yl)carbamate (1 equiv) was dissolved in CH_2Cl_2 (0.1 M) and cooled to 0 °C. Trifluoroacetic acid (0.2M) was added, and the reaction mixture was stirred for 1 h. The starting material was determined to be consumed by TLC, and the reaction mixture was concentrated, resulting in a brown oil. The resulting (*R*)-3-amino-2-methylbutan-2-ol TFA salt was dissolved in DMF (0.2 M) and used without purification.

(*R*)-5-Bromo-*N*-(3-hydroxy-3-methylbutan-2-yl)picolinamide (30). In a scintillation vial, (*R*)-*tert*-butyl (3-hydroxy-3-methylbutan-2-yl)carbamate (1.5 g, 7.4 mmol, 1 equiv) was dissolved in CH_2Cl_2 (6 mL, 0.12 M) and cooled to 0 °C. Trifluoroacetic acid (3 mL, 0.25 M) was added, and the reaction mixture was stirred for 1 h. The starting material was determined to be consumed by TLC, and the reaction

mixture was concentrated via rotary evaporation resulting in a brown oil. The resulting (*R*)-3-amino-2-methylbutan-2-ol TFA salt was dissolved in DMF (5 mL) and used without purification. In a 100 mL round-bottom flask 5-bromopicolinic acid (1.49 g, 7.4 mmol, 1.0 equiv) and HATU (3.1 g, 8.14 mmol, 1.1 equiv) were combined in DMF (25 mL, 0.3 M). *N*,*N*-Diisopropylethylamine (3.2 mL, 18.25 mmol, 5 equiv) was then added, and the reaction was stirred for 15 min. The (*R*)-3-amino-2-methylbutan-2-ol TFA salt was added as a solution in DMF, and the reaction was stirred 18 h after which the reaction was determined to be complete by LC−MS. The reaction mixture was partitioned between EtOAc (75 mL) and H_2O (25 mL). After separating the aqueous layer the organic layer was washed again with H_2O (2 × 15 mL). The organic layer was then dried with Na_2SO_4, concentrated, and purified via silica gel chromatography eluting with Hex/EtOAc (0−75% EtOAc) with the aryl bromide eluting at 40% EtOAc. The product was isolated as a brown oil (1.72 g, 81% yield). $[\alpha]^{20}_D$ = −13.7 (*c* 0.81, $CHCl_3$); ^{1}H NMR (400 MHz, $CDCl_3$) δ 8.51 (1H, bs), 8.09 (1H, d, *J* = 9.2 Hz), 8.01 (1H, m), 7.90 (1H, m), 4.04 (1H, m), 3.03 (1H, bs), 1.22 (9 H,bs); ^{13}C NMR (100 MHz, $CDCl_3$) δ 163.4, 149.1, 148.2, 139.8, 123.7, 123.6,72.6, 53.5, 27.4, 25.8, 15.7; HRMS (ES+, M + Na) calcd for $C_{11}H_{15}N_2O_2BrNa$ 309.0215, found 309.0212.

General Methods for Series 31. Method A, 31a−n. In a scintillation vial, (*R*)-5-bromo-*N*-(3-hydroxy-3-methylbutan-2-yl)-picolinamide, **31**, (1 equiv) was placed under argon atmosphere and dissolved in DMF (0.25M). $PdCl_2(PPh_3)_2$ (0.05 equiv) and CuI (0.1 equiv) were added, followed by an alkyne (1.25 equiv) and Et_2NH (6 equiv). The reaction mixture was heated to 90 °C for 45 min after which the reaction was determined to be complete by LC−MS. The reaction mixture was filtered through a Fisherbrand Nylon 0.45 μm syringe filter and purified directly by preparative RP-HPLC eluting with 0.1% TFA in H_2O/MeCN (10−90% MeCN).

Method B, 31o−r. In a scintillation vial, (*R*)-5-ethynyl-*N*-(3-hydroxy-3-methylbutan-2-yl)picolinamide, **33**, (1 equiv) was placed under argon atmosphere and dissolved in DMF (0.25M). An aryl halide (1 equiv), $Pd(PPh_3)_4$ (0.05 equiv) and CuI (0.1 equiv) were added, followed by Et_3N (17 equiv). The reaction mixture heated to 60 °C until the reaction was determined to be complete by LC−MS (1−2 h). The reaction mixture was filtered through a Fisherbrand Nylon 0.45 μm syringe filter and purified directly by preparative RP-HPLC eluting with 0.1% TFA in H_2O/MeCN (10−90% MeCN).

(*R*)-5-((3-Fluorophenyl)ethynyl)-*N*-(3-hydroxy-3-methylbutan-2-yl)-3-methylpicolinamide (31d). LC−MS: t_R = 0.798 min, >98% at 215 and 254 nm, *m*/*z* = 341.2 [M + H]$^+$. $[\alpha]^{20}_D$ = −14.2 (*c* 0.74, $CHCl_3$); ^{1}H NMR (400 MH, $CDCl_3$) δ 8.48 (1H, d, *J* = 1.6 Hz), 8.24 (1H, d, *J* = 8.8 Hz), 7.70 (1H, d, *J* = 1.2 Hz), 7.32 (2H, m), 7.24 (1H, m), 7.10 (1H, m), 4.10 (1H, dq, *J* = 8.9, 6.9 Hz), 2.73 (3H, s), 2.68 (1H, bs), 1.27 (9H, m); ^{13}C NMR (100 MHz, $CDCl_3$) δ 165.6, 162.3 (d, J_{C-F} = 245.6 Hz), 147.6, 146.0, 143.0, 135.0, 130.1 (d, J_{C-F} = 8.6 Hz), 127.6 (d, J_{C-F} = 3.0 Hz), 124.0 (d, J_{C-F} = 9.4 Hz), 121.8, 118.5 (d, J_{C-F} = 22.8 Hz), 116.4 (d, J_{C-F} = 21.1 Hz), 92.8, 86.2, 73.1, 53.4, 27.6, 25.5, 20.3, 16.0; HRMS (ES+, M + H) calcd for $C_{20}H_{22}FN_2O_2$ 341.1665, found 341.1663.

(*R*)-*N*-(3-Hydroxy-3-methylbutan-2-yl)-5-(pyridin-2-ylethynyl)picolinamide (31i). LC−MS: t_R = 0.533 min, >98% at 215 and 254 nm, *m*/*z* = 310.2 [M + H]$^+$. $[\alpha]^{20}_D$ = −21.1 (*c* 0.53, $CHCl_3$); ^{1}H NMR (400 MHz, $CDCl_3$) δ 8.71 (1H, bs), 8.64 (1H, d, *J* = 4.6 Hz), 8.17 (2H, d, *J* = 8.1 Hz), 7.99 (1H, dd, *J* = 8.1, 1.7 Hz), 7.71 (1H, dt, *J* = 7.8, 1.5 Hz), 7.55 (1H, d, *J* = 7.9 Hz), 7.28 (1H, m), 4.11 (1H, dq, *J* = 8.9, 6.7 Hz), 2.70 (1H, bs), 1.27 (3H, d, *J* = 6.8 Hz), 1.26 (6H, d, *J* = 8.1 Hz); ^{13}C NMR (100 MHz, $CDCl_3$) δ 163.7, 150.7, 150.2, 148.8, 142.4, 140.1, 136.3, 127.4, 123.4, 121.9, 121.7, 93.4, 85.1, 72.9, 53.7, 27.6, 25.8, 15.9; HRMS (ES+, M + H) calcd for $C_{18}H_{20}N_3O_2$ 310.1556, found 310.1554.

(*R*)-*N*-(3-Hydroxy-3-methylbutan-2-yl)-5-(pyridin-4-ylethynyl)picolinamide (31k). LC−MS: t_R = 0.461 min, >98% at 215 and 254 nm, *m*/*z* = 310.2 [M + H]$^+$. $[\alpha]^{20}_D$ = −27.8 (*c* 0.48, $CHCl_3$); ^{1}H NMR (400 MHz, $CDCl_3$) δ 8.67 (1H, dd, *J* = 1.6 Hz), 8.65 (1H, bs), 8.20 (1H, m), 8.17 (1H, bs), 7.97 (1H, dd, *J* = 8.2, 2.0 Hz), 7.41 (2H, d, *J* = 4.9 Hz), 4.12 (1H, dq, *J* = 9.5, 7.0 Hz), 2.59 (1H, bs), 1.29 (3H, d, *J* = 6.9 Hz), 1.28 (6H, d, *J* = 5.6 Hz); ^{13}C NMR (100 MHz, $CDCl_3$) δ 163.6, 150.6, 149.8, 149.0, 140.1, 130.3, 125.6, 121.8, 121.7, 91.5, 89.8, 72.9, 53.7, 27.6, 25.8, 15.9; HRMS (ES+, M + H) calcd for $C_{18}H_{20}N_3O_2$ 310.1556, found 310.1554.

(*R*)-5-Ethynyl-*N*-(3-hydroxy-3-methylbutan-2-yl)-picolinamide (33). In a 100 mL round-bottom flask, (*R*)-5-bromo-*N*-(3-hydroxy-3-methylbutan-2-yl)picolinamide (1.5 g, 5.2 mmol, 1 equiv), $PdCl_2(PPh_3)_2$ (187 mg, 026 mmol, 0.05 equiv), and CuI (99 mg, 0.52 mmol, 0.1 equiv) were combined, placed under argon atmosphere, and dissolved in DMF (15 mL, 0.35M). Trimethylsilylacetylene (1.1 mL, 7.8 mmol, 1.5 equiv) was added, followed by Et_2NH (3.2 mL, 31.2 mmol, 6 equiv). The reaction mixture heated to 90 °C for 45 min after which the reaction was determined to be complete by LC−MS. The reaction mixture was diluted with EtOAc (45 mL) and washed with H_2O (3 × 15 mL). The organic layer was dried with Na_2SO_4, concenterated, and purified via silica gel chromatography eluting with Hex/EtOAc (0 to 75% EtOAc) with the trimethylsilyl-protected acetylene eluting at 40% EtOAc as a pale yellow oil (1.22 g, 77% yield). ^{1}H NMR (400 MHz, $CDCl_3$) δ8.55 (1H, bs), 8.10 (1H, d, *J* = 9.1 Hz), 8.14 (1H, dd, *J* = 8.1, 1.8 Hz), 7.85 (1H, dd, *J* = 8.1, 2.0 Hz), 4.10 (1H, m), 2.65 (1H, bs), 1.27 (3H, d, *J* = 7.7 Hz), 1.26 (6H, d, *J* = 5.8 Hz), 0.26 (9H, s).

The trimethylsilyl-protected acetylene (1.22 g, 4.0 mmol, 1 equiv) was dissolved in MeOH/THF (1:1, 16 mL, 0.25 M), and K_2CO_3 (1.1 g, 8.0 mmol, 2 equiv) was added. The reaction was stirred at room temperature for 1 h after which it was determined to be complete by LC−MS. The reaction mixture was diluted with H_2O (5 mL) and extracted with EtOAc (3 × 20 mL). The organic layer was dried with Na_2SO_4, cocentrated, and purified via silica gel chromatography eluting with Hex/EtOAc (0 to 100% EtOAc) with the acetylene eluting at 60−80% EtOAc as a pale yellow oil (883 mg, 95% yield). $[\alpha]^{20}_D$ = −4.9 (*c* 0.73, $CHCl_3$); ^{1}H NMR (400 MHz, $CDCl_3$) δ 8.61 (1H, d, *J* = 1.2 Hz), 8.17 (1H, bs), 8.14 (1H, dd, *J* = 8.0, 0.3 Hz), 7.90 (1H, dd, *J* = 8.1, 2.0 Hz), 4.10 (1H, dq, *J* = 9.1, 6.9 Hz), 3.34 (1H, s), 2.58 (1H, s), 1.27 (3H, d, *J* = 6.9 Hz), 1.26 (6H, d, *J* = 5.8 Hz); ^{13}C NMR (100 MHz, $CDCl_3$) δ 163.7, 151.0, 148.8, 140.4, 121.8, 121.7, 82.7, 79.9, 73.0, 53.7, 27.6, 25.7, 15.9; HRMS (ES+, M + Na) calcd for $C_{13}H_{16}N_2O_2Na$ 255.1109, found 255.1107.

General Methods for Series 36. Method A, 36a,b,d,e,h−j. In a scintillation vial, an aryl halide carboxylic acid, **34a** (1 equiv), $PdCl_2(PPh_3)_2$ (0.05 equiv), and CuI (0.1 equiv) were combined, placed under argon atmosphere, and dissolved in DMF (0.25M). 3-Fluorophenylacetylene (1.25 equiv) was added, followed by Et_2NH (6 equiv). The reaction mixture was heated to 90 °C for 45 min after which the reaction was determined to be complete by LC−MS. The reaction mixture was filtered through a Fisherbrand Nylon 0.45 μm syringe filter and purified directly by preparative RP-HPLC eluting with 0.1% TFA in H_2O/MeCN (10−90% MeCN) to yield the desired acetylene carboxylic acid **35a**.

In a scintillation vial, acetylene carboxylic acid **35a** (1.0 equiv) and HATU (1.1 equiv) were combined in DMF (0.25 M). *N*,*N*-Diisopropylethylamine (DIPEA, 5 equiv) was then added. After the reaction mixture was stirred for 10 min, a solution of freshly prepared (*R*)-3-amino-2-methylbutan-2-ol TFA salt in DMF (1.1 equiv) was added, and the reaction was stirred until determined to be complete by LC−MS (2−20 h). The reaction mixture was filtered through a Fisherbrand Nylon 0.45 μm syringe filter and purified directly by preparative RP-HPLC eluting with 0.1% TFA in H_2O/MeCN (10−90% MeCN).

Method B, 36c,f,g. In a scintillation vial an aryl halide carboxylic ester, **34b** (1 equiv), $Pd(PPh_3)_4$ (0.05 equiv), and CuI (0.1 equiv) were combined, placed under an argon atmosphere, and dissolved in DMF (0.25 M). 3-Fluorophenylacetylene (1.25 equiv) was added, followed by Et_3N (17 equiv). The reaction mixture heated to 60 °C until the reaction was determined to be complete by LC−MS (1−2 h). The reaction mixture was filtered through a Fisherbrand Nylon 0.45 μm syringe filter and purified directly by preparative RP-HPLC eluting with 0.1% TFA in H_2O/MeCN (10−90% MeCN) to yield the desired acetylene carboxylic ester **35b**.

Methyl or ethyl ester **35b** (1 equiv) was dissolved in THF/H_2O (4:1, 0.1 M), and LiOH (3 equiv) was added. The reaction was vigorously stirred until the starting material was observed to be consumed by LC−MS (30 min to 16 h). The reaction was quenched with 2 M HCl and extracted with ethyl acetate (3 × 10 mL). The organic layers were combined, dried with Na_2SO_4, concentrated, and used without further purification. In a scintillation vial, the resulting acetylene carboxylic acid (1.0 equiv) and HATU (1.1 equiv) were combined in DMF (0.25 M). *N,N*-Diisopropylethylamine (DIPEA, 5 equiv) was then added. After the reaction mixture was stirred for 10 min, a solution of freshly prepared (*R*)-3-amino-2-methylbutan-2-ol TFA salt in DMF (1.1 equiv) was added, and the reaction was stirred until determined to be complete by LC−MS (2−20 h). The reaction mixture was filtered through a Fisherbrand Nylon 0.45 μm syringe filter and purified directly by preparative RP-HPLC eluting with 0.1% TFA in H_2O/MeCN (10−90% MeCN).

(*R*)-6-((3-Fluorophenyl)ethynyl)-*N*-(3-hydroxy-3-methylbutan-2-yl)nicotinamide (36b). LC−MS: t_R = 0.765 min, >98% at 215 and 254 nm, m/z = 326.9 [M + H]$^+$. $[\alpha]^{20}_D$ = −7.5 (*c* 0.57, $CHCl_3$); ^{1}H NMR (400 MHz, $CDCl_3$) δ 8.98 (1H, d, *J* = 1.8 Hz), 8.10 (1H, dd, *J* = 8.1, 2.3 Hz), 7.55 (1H, d, *J* = Hz), 7.32 (3H, m), 7.08 (1H, m), 6.76 (1H, d, *J* = 8.8 Hz), 4.13 (1H, dq, *J* = 8.8, 6.8 Hz), 2.62 (1H, bs), 1.29 (6H, d, *J* = 4.4 Hz), 1.27 (3H, d, *J* = 6.8 Hz); ^{13}C NMR (100 MHz, $CDCl_3$) δ 164.8, 162.3 (d, J_{C-F} = 245 Hz), 148.3, 145.3, 135.3, 130.1 (d, J_{C-F} = 8.5 Hz), 129.1, 128.0 (d, J_{C-F} = 7.0 Hz), 126.9, 123.5 (d, J_{C-F} = 9.4 Hz), 118.8 (d, J_{C-F} = 23.0), 116.8 (d, J_{C-F} = 21.0 Hz), 90.0 (d, J_{C-F} = 3.4 Hz), 88.7, 72.6, 53.7, 28.0, 26.3, 15.7 ; HRMS (ES+, M + H) calcd for $C_{19}H_{20}FN_2O_2$: 327.1509, found 327.1510.

(*R*)-6-((3-Fluorophenyl)ethynyl)-*N*-(3-hydroxy-3-methylbutan-2-yl)-5-methylnicotinamide (36e). LC−MS: t_R = 0.816 min, >98% at 215 and 254 nm, m/z = 341.2 [M + H]$^+$. $[\alpha]^{20}_D$ = −17.9 (*c* 0.43, $CHCl_3$); ^{1}H NMR (400 MH, $CDCl_3$) δ 8.57 (1H, s), 8.17 (1H, d, *J* = 7.2 Hz), 8.07 (1H, s), 7.36 (2H, s), 7.24 (1H, m), 7.09 (1H, m), 4.12 (1H, dq, *J* = 8.9, 6.9 Hz), 2.55 (3H, s), 1.71 (1H, bs), 1.29 (3H, d, *J* = 6.8 Hz), 1.28 (6H, d *J* = 9.0 Hz); ^{13}C NMR (100 MHz, $CDCl_3$) δ 164.2, 162.4 (d, J_{C-F} =245.7 Hz), 150.6, 150.5, 148.2, 130.1 (d, J_{C-F} = 8.6 Hz), 127.6 (d, J_{C-F} = 3.0 Hz), 124.2 (d, J_{C-F} = 9.2 Hz), 122.9, 122.6, 118.6 (d, J_{C-F} = 22.7 Hz), 116.4 (d, J_{C-F} = 21.1 Hz), 96.8, 85.4, 73.1, 53.8, 27.6, 25.6, 20.4, 15.9; HRMS (ES+, M + H) calcd for $C_{20}H_{22}FN_2O_2$ 341.1665, found 341.1664.

(*R*)-2-((3-Fluorophenyl)ethynyl)-*N*-(3-hydroxy-3-methylbutan-2-yl)pyrimidine-5-carboxamide (36f). LC−MS: t_R = 0.708 min, >98% at 215 and 254 nm, m/z = 327.9 [M + H]$^+$. $[\alpha]^{20}_D$ = −8.9 (*c* 0.67, $CHCl_3$); ^{1}H NMR (400 MHz, $CDCl_3$) δ 9.12 (2H, s), 7.43 (1H, d, *J* = 7.8 Hz), 7.34 (2H, m), 7.14 (1H, td, *J* = 9.2, 2.4 Hz), 6.75 (1H, d, *J* = 8.8 Hz), 4.14 (1H, dq, *J* = 8.8, 6.9 Hz), 2.31 (1H, bs), 1.30 (6H, s), 1.28 (3H, d, *J* = 6.9 Hz); ^{13}C NMR (100 MHz, $CDCl_3$) δ 162.8, 162.2 (d, J_{C-F} = 246.1 Hz), 156.1, 154.3, 130.2 (d, J_{C-F} = 8.4 Hz), 128.6 (d, J_{C-F} = 3.1 Hz), 125.9, 122.6 (d, J_{C-F} = 9.4 Hz), 119.4 (d, J_{C-F} = 23.1 Hz), 117.5 (d, J_{C-F} = 21.2 Hz), 88.6 (d, J_{C-F} = 3.5 Hz), 88.2, 72.5, 53.7, 28.0, 26.4, 15.7; HRMS (ES+, M + H) calcd for $C_{18}H_{19}FN_3O_2$ 328.1461, found 328.1459.

5-((3-Fluorophenyl)ethynyl)-*N*-(3-hydroxy-3-methylbutyl)picolinamide (38p). LC−MS: t_R = 0.870 min, >98% at 215 and 254 nm, m/z = 326.9 [M + H]$^+$. ^{1}H NMR (400 MHz, $CDCl_3$) δ 8.61 (1H, bs), 8.42 (1H, m), 8.15 (1H, d, *J* = 8.1 Hz), 7.90 (1H, dd, *J* = 8.1, 2.0 Hz), 7.31 (2H, m), 7.22 (1H, m), 7.07 (1H, m), 3.63 (2H, q, *J* = 6.1 Hz), 2.44 (1H, bs), 1.82 (2H, t, *J* = 7.0 Hz), 1.30 (6H, s); ^{13}C NMR (100 MHz, $CDCl_3$) δ 163.8, 162.3 (d, J_{C-F} = 245.7 Hz), 150.4, 148.7, 139.7, 130.1 (d, J_{C-F} = 8.6 Hz), 127.6 (d, J_{C-F} = 3.1 Hz), 123.9 (d, J_{C-F} = 9.4 Hz),122.7, 121.5, 118.5 (d, J_{C-F} = 22.8 Hz), 116.4 (d, J_{C-F} = 21.1 Hz), 93.1 (d, J_{C-F} = 3.5 Hz), 86.3, 70.5, 42.0, 35.8, 29.6; HRMS (ES+, M + H) calcd for $C_{19}H_{20}FN_2O_2$ 327.1509, found 327.1508.

(*R*)-5-((3-Fluorophenyl)ethynyl)-*N*-(1,1,1-trifluoropropan-2-yl)picolinamide (38r). LC−MS: t_R = 1.030 min, >98% at 215 and 254 nm, m/z = 336.9 [M + H]$^+$. $[\alpha]^{20}_D$ = 10.5 (*c* 0.59, $CHCl_3$); ^{1}H NMR (400 MHz, $CDCl_3$) δ 8.68 (1H, d, *J* = 1.4 Hz), 8.20 (1H, d, *J* = 8.1 Hz), 8.11 (1H, d, *J* = 9.8 Hz), 7.97 (1H, dd, *J* = 7.8, 1.8 Hz), 7.35 (2H, m), 7.27 (1H, m), 7.10 (1H, m), 4.88 (1H, m), 1.46 (3H, d, *J* = 7.0 Hz); ^{13}C NMR (100 MHz, $CDCl_3$) δ 163.3, 162.4 (d, J_{C-F} = 245.7 Hz), 150.5, 147.4, 139.9, 130.2 (d, J_{C-F} = 8.6 Hz), 127.7 (d, J_{C-F} = 3.1 Hz), 125.3 (q, J_{C-F} = 279.3 Hz), 123.8 (d, J_{C-F} = 9.4 Hz), 123.2, 122.0, 118.6 (d, J_{C-F} = 22.9 Hz), 116.6 (d, J_{C-F} = 21.0 Hz), 93.7, 86.1, 46.5 (q, J_{C-F} = 31.6 Hz), 14.4 (d, J_{C-F} = 1.5 Hz); HRMS (ES+, M + H) calcd for $C_{17}H_{13}F_4N_2O$ 337.0964, found 337.0966.

(*S*)-5-((3-Fluorophenyl)ethynyl)-*N*-(1,1,1-trifluoropropan-2-yl)picolinamide (38s). LC−MS: t_R = 1.030 min, >98% at 215 and 254 nm, m/z = 336.9 [M + H]$^+$. $[\alpha]^{20}_D$ = −10.0 (*c* 0.82, $CHCl_3$); ^{1}H NMR (400 MHz, $CDCl_3$) δ 8.68 (1H, d, *J* = 1.4 Hz), 8.20 (1H, d, *J* = 8.1 Hz), 8.11 (1H, d, *J* = 9.8 Hz), 7.97 (1H, dd, *J* = 7.8, 1.8 Hz), 7.35 (2H, m), 7.27 (1H, m), 7.10 (1H, m), 4.88 (1H, m), 1.46 (3H, d, *J* = 7.0 Hz); ^{13}C NMR (100 MHz, $CDCl_3$) δ 163.3, 162.4 (d, J_{C-F} = 245.7 Hz), 150.5, 147.4, 139.9, 130.2 (d, J_{C-F} = 8.6 Hz), 127.7 (d, J_{C-F} = 3.1 Hz), 125.3 (q, J_{C-F} = 279.3 Hz), 123.8 (d, J_{C-F} = 9.4 Hz), 123.2, 122.0, 118.6 (d, J_{C-F} = 22.9 Hz), 116.6 (d, J_{C-F} = 21.0 Hz), 93.7, 86.1, 46.5 (q, J_{C-F} = 31.6 Hz), 14.4 (d, J_{C-F} = 1.5 Hz); HRMS (ES+, M + H) calcd for $C_{17}H_{13}F_4N_2O$ 337.0963.

5-((3-Fluorophenyl)ethynyl)-*N*-(3-methyloxetan-3-yl)picolinamide (38t). LC−MS: t_R = 0.879 min, >98% at 215 and 254 nm, m/z = 310.9 [M + H]$^+$. ^{1}H NMR (400 MHz, $CDCl_3$) δ 8.64 (1H, d, *J* = 1.4 Hz), 8.29 (1H, bs), 8.13 (1H, d, *J* = 7.8 Hz), 7.93 (1H, dd, *J* = 8.1, 2.0 Hz), 7.33 (2H, m), 7.24 (1H, m), 7.09 (1H, m), 4.94 (2H, d, *J* = 6.4 Hz), 4.57 (2H, d, *J* = 6.5 Hz), 1.77 (3H, s); ^{13}C NMR (100 MHz, $CDCl_3$) δ 162.9, 162.3 (d, J_{C-F} = 245.9 Hz), 150.4, 148.2, 139.8, 130.1 (d, J_{C-F} = 8.6 Hz), 127.6 (d, J_{C-F} = 3.0 Hz), 123.8 (d, J_{C-F} = 9.3 Hz), 122.7, 121.3, 118.5 (d, J_{C-F} = 22.9 Hz), 116.5 (d, J_{C-F} = 21.0 Hz), 93.5 (d, J_{C-F} = 3.5 Hz), 86.2, 81.8, 53.6, 23.6; HRMS (ES+, M + H) calcd for $C_{18}H_{16}FN_2O_2$ 311.1196, found 311.1197.

5-((3-Fluorophenyl)ethynyl)-*N*-((3-methyloxetan-3-yl)methyl)picolinamide (38u). LC−MS: t_R = 0.797 min, >98% at 215 and 254 nm, m/z = 325.1 [M + H]$^+$. ^{1}H NMR (400 MHz, $CDCl_3$) δ 8.67 (1H, d, *J* = 1.3 Hz), 8.29 (1H, bs), 8.20 (1H, d, *J* = 7.6 Hz), 7.97 (1H, dd, *J* = 6.0, 2.0 Hz), 7.35 (2H, m), 7.26 (1H, m), 7.10 (1H, m), 4.59 (2H, d, *J* = 6.0 Hz), 4.44 (2H, d, *J* = 6.0 Hz), 3.68 (2H, d, *J* = 6.5 Hz), 1.40 (3H, s); ^{13}C NMR (100 MHz, $CDCl_3$) δ 164.2, 162.4 (d, J_{C-F} = 245.9 Hz), 150.5, 148.2, 139.9, 130.2 (d, J_{C-F} = 8.7 Hz), 127.7 (d, J_{C-F} = 3.0 Hz), 123.9 (d, J_{C-F} = 9.4 Hz), 122.7, 121.8, 118.6 (d, J_{C-F} = 22.8 Hz), 116.6 (d, J_{C-F} = 21.1 Hz), 93.4 (d, J_{C-F} = 3.7 Hz), 86.3, 80.3, 45.9, 40.2, 22.0; HRMS (ES+, M + H) calcd for $C_{19}H_{18}FN_2O_2$ 325.1352, found 325.1353.

5-((3-Fluorophenyl)ethynyl)picolinic Acid (37). In a 100 mL round-bottom flask, 5-bromopicolinic acid (3g, 14.8 mmol, 1 equiv), $PdCl_2(PPh_3)_2$ (519 mg, 0.74 mmol, 0.05 equiv), and CuI (282 mg, 1.48 mmol, 0.1 equiv) were combined, place under an argon atmosphere, and dissolved in DMF (50 mL, 0.3 M). 3-Fluorophenylacetylene (2.05 mL, 17.76 mmol, 1.2 equiv) was added, followed by Et_2NH (9.2 mL, 88.8 mmol, 6 equiv). The reaction mixture heated to 90 °C for 45 min after which the reaction was determined to be complete by LC−MS. The crude reaction mixture was diluted with EtOAc (50 mL) and H_2O (50 mL). After separating the organic layer, the aqueous layer was washed with EtOAc (2 × 25 mL). The aqueous layer was then acidified to ∼pH = 2 with 2 M HCl, and extracted with EtOAc (3 × 50 mL). The organic layer was dried with Na_2SO_4, concentrated, and used without further purification. The product was isolated as a white solid (2.32 g, 65%). ^{1}H NMR (400 MHz, CD_3OD) δ 8.81 (1H, bs), 8.16 (2H, m), 7.44 (2H, m), 7.34 (1H, d, *J* = 9.7 Hz), 7.21 (1H, m); ^{13}C NMR (100 MHz, CD_3OD) δ 167.0, 163.9 (d, J_{C-F} = 244.4 Hz), 152.5, 148.0, 141.3, 131.7 (d, J_{C-F} = 8.6 Hz), 129.0, 125.8, 125.2 (d, J_{C-F} = 9.3 Hz), 124.8, 119.4 (d, J_{C-F} = 23.4 Hz), 117.7 (d, J_{C-F} = 21.4 Hz), 94.8, 86.8; HRMS (ES+, M + H) calcd for $C_{14}H_9FNO_2$ 242.0617, found 242.0618.

Amide Analogues 19, 38a−d,g−v. In a scintillation vial, 5-((3-fluorophenyl)ethynyl)picolinic acid, **37**, (1.0 equiv) and HATU (1.1 equiv) were combined in DMF (0.25 M). *N,N*-Diisopropylethylamine (DIPEA, 3 equiv) was then added. The reaction mixture was stirred for 10 min after which an amine (1.1 equiv) was added. The reaction was stirred until determined to be complete by LC−MS (2−20 h). The reaction mixture was filtered through a Fisherbrand Nylon 0.45 μm syringe filter and purified directly by preparative RP-HPLC eluting with 0.1% TFA in H_2O/MeCN (10−90% MeCN).

(*R*)-5-((3-Fluorophenyl)ethynyl)-*N*-(3-hydroxy-3-methylbutan-2-yl)picolinamide (19). LC−MS: t_R = 0.731 min, >98% at 215 and 254 nm, m/z = 327.1 [M + H]$^+$. $[\alpha]^{20}_D$ = −22.2 (*c* 0.43, $CHCl_3$); ^{1}H NMR (400 MHz, $CDCl_3$) δ 8.65 (1H, dd, *J* = 1.3, 0.7 Hz), 8.19 (2H, dd, *J* = 8.1, 0.7 Hz), 7.95 (1H, dd, *J* = 8.1, 2.0 Hz), 7.34 (2H, m), 7.24 (1H, m), 7.09 (1H, m), 4.13 (1H, dq, *J* = 9.1, 6.8 Hz), 2.50 (1H, bs), 1.29 (3H, d, *J* = 6.8 Hz), 1.28 (6H, d, *J* = 8.0 Hz); ^{13}C NMR (100 MHz, $CDCl_3$) δ 163.8 162.3 (d, J_{C-F} = 245.7 Hz), 150.4, 148.4, 139.8, 130.1 (d, J_{C-F} = 8.6 Hz), 127.7 (d, J_{C-F} = 3.0 Hz), 123.9 (d, J_{C-F} = 9.3 Hz), 122.5, 121.8, 118.5 (d, J_{C-F} = 22.9 Hz), 116.5 (d, J_{C-F} = 21.0 Hz), 93.3, 86.3, 73.1, 53.8, 27.6, 25.7, 15.9; HRMS (ES+, M + H) calcd for $C_{19}H_{20}FN_2O_2$ 327.1509, found 327.1507.

(*R*)-*N*-(3-Fluoro-3-methylbutan-2-yl)-5-((3-fluorophenyl)-ethynyl)picolinamide (38e). (*R*)-5-((3-Fluorophenyl)ethynyl)-*N*-(3-hydroxy-3-methylbutan-2-yl)picolinamide, **19**, (40 mg, 0.12 mmol, 1.0 equiv) was dissolved in CH_2Cl_2 (1.2 mL, 0.1 M) and cooled to −78 °C. DAST (19 μL, 0.12 mmol, 1.0 equiv) was added dropwise, and the reaction was allowed to slowly warm to rt over 4 h. The reaction was determined to be complete by LC−MS and was quenched carefully by the addition of H_2O (0.5 mL). The aqueous layer was extracted with EtOAc (3 × 5 mL), dried Na_2SO_4, concentrated, and purified by preparative RP-HPLC eluting with 0.1% TFA in H_2O/MeCN (10−90% MeCN) to afford the title compound in 30% yield. LC−MS: t_R = 0.926 min, >98% at 215 and 254 nm, m/z = 329.1 [M + H]$^+$. $[\alpha]^{20}_D$ = −5.9 (*c* 1.16, $CHCl_3$); ^{1}H NMR (400 MHz, $CDCl_3$) δ 8.68 (1H, d, *J* = 1.3 Hz), 8.19 (1H, dd, *J* = 12.0, 0.4 Hz), 8.14 (1H, d, *J* = 9.8 Hz), 7.96 (1H, dd, *J* = 8.1, 2.0 Hz), 7.35 (2H, m), 7.27 (1H, m), 7.10 (1H, m), 4.29 (1H, m), 1.57 (1H, bs), 1.46 (3H, d, *J* = 16.7 Hz), 1.40 (3H, d, *J* = 16.7 Hz), 1.33 (3H, d, *J* = 6.9 Hz); ^{13}C NMR (100 MHz, $CDCl_3$) δ 163.2, 162.4 (d, J_{C-F} = 22.9 Hz), 150.5, 148.4, 139.8, 130.1 (d, J_{C-F} = 8.7 Hz), 127.7 (d, J_{C-F} = 3.2 Hz), 124.0 (d, J_{C-F} = 9.4 Hz), 122.6, 121.8, 118.6 (d, J_{C-F} = 21.8 Hz), 116.5, (d, J_{C-F} = 21.0 Hz), 96.6 (d, J_{C-F} = 170.7 Hz), 93.3 (d, J_{C-F} = 3.4 Hz), 86.4, 51.8 (d, J_{C-F} = 22.2 Hz), 24.6 (d, J_{C-F} = 7.8 Hz), 24.3 (d, J_{C-F} = 7.4 Hz), 15.6 (d, J_{C-F} = 3.7 Hz) ; HRMS (ES+, M + H) calcd for $C_{19}H_{18}F_2N_2ONa$ 351.1285, found 351.1282.

(*R*)-5-((3-Fluorophenyl)ethynyl)-*N*-(3-methoxy-3-methylbutan-2-yl)picolinamide (38f). (*R*)-5-((3-Fluorophenyl)ethynyl)-*N*-(3-hydroxy-3-methylbutan-2-yl)picolinamide, **19**, (68 mg, 0.21 mmol, 1.0 equiv) was dissolved in THF (2 mL, 0.1 M) and cooled to 0 °C. NaH (11.1 mg, 0.46 mmol, 2.2 equiv) was added. The reaction mixture was warmed to rt and stirred for 10 min. Methyl iodide (15 μL, 0.23 mmol, 1.1 equiv) was added, and the reaction mixture was stirred at room temperature overnight. Analysis of the reaction mixture by LC−MS revealed ∼70% of the desired product, ∼20% starting material, and ∼10% dimethylated product. The reaction was quenched with NH_4Cl (satd, aq) and extracted with EtOAc (3 × 5 mL). The organic layers were dried with Na_2SO_4, concentrated, and purified by preparative RP-HPLC eluting with 0.1% TFA in H_2O/MeCN (10−90% MeCN) to afford the product in 58% yield. LC−MS: t_R = 0.824 min, >98% at 215 and 254 nm, m/z = 341.2 [M + H]$^+$. $[\alpha]^{20}_D$ = −31.7 (*c* 0.65, $CHCl_3$); ^{1}H NMR (400 MHz, $CDCl_3$) δ 8.66 (1H, d, *J* = 1.6 Hz), 8.21 (1H, d, *J* = 9.6 Hz), 8.17 (1H, d, *J* = 8.1 Hz), 7.92 (1H, dd, *J* = 8.1, 1.9 Hz), 7.32 (2H, m), 7.23, (1H, m), 7.07 (1H, m), 4.18 (dq, 1H, *J* = 9.5, 6.7 Hz), 3.25 (3H, s), 1.23 (3H, d, *J* = 6.9 Hz), 1.20 (6H, d, *J* = 11.6 Hz), ; ^{13}C NMR (100 MHz, $CDCl_3$) δ 163.0, 162.3 (d, J_{C-F} = 245.6 Hz), 150.4, 148.8, 139.6, 130.1 (d, J_{C-F} = 8.6 Hz), 127.6 (d, J_{C-F} = 3.0 Hz), 124.0 (d, J_{C-F} = 9.3 Hz), 122.2, 121.6, 118.5 (d, J_{C-F} = 22.9 Hz), 116.4 (d, J_{C-F} = 21.1 Hz), 93.0, 86.4, 75.9, 52.3, 49.4, 22.0, 21.9, 15.5; HRMS (ES+, M + H) calcd for $C_{20}H_{22}FN_2O_2$ 341.1665, found 341.1664.

(*S*)-5-((3-Fluorophenyl)ethynyl)-*N*-(3-hydroxy-3-methylbutan-2-yl)picolinamide (38l). LC−MS: t_R = 0.738 min, >98% at 215 and 254 nm, m/z = 327.1 [M + H]$^+$. $[\alpha]^{20}_D$ = 24.3 (*c* 0.48, $CHCl_3$); ^{1}H NMR (400 MHz, $CDCl_3$) δ 8.64 (1H, dd, *J* = 1.3, 0.7 Hz), 8.19 (1H, bs), 8.18 (1H, dd, *J* = 8.1, 0.7 Hz), 7.94 (1H, dd, *J* = 8.1, 2.0 Hz), 7.34 (2H, m), 7.24 (1H, m), 7.09 (1H, m), 4.13 (1H, dq, *J* = 9.1, 6.8 Hz), 2.66 (1H, bs), 1.29 (3H, d, *J* = 6.8 Hz), 1.28 (6H, d, *J* = 8.0 Hz); ^{13}C NMR (100 MHz, $CDCl_3$) δ 163.8 162.3 (d, J_{C-F} = 245.7 Hz), 150.4, 148.4, 139.8, 130.1 (d, J_{C-F} = 8.6 Hz), 127.6 (d, J_{C-F} = 3.0 Hz), 123.9 (d, J_{C-F} = 9.3 Hz), 122.5, 121.8, 118.5 (d, J_{C-F} = 22.9 Hz), 116.5 (d, J_{C-F} = 21.0 Hz), 93.3, 86.3, 73.1, 53.7, 27.6, 25.7, 15.9; HRMS (ES +, M + H) calcd for $C_{19}H_{20}FN_2O_2$ 327.1509, found 327.1507.

General Amide Coupling and Sonogashira Two-Step Procedure (44a,b,d, 45). In a scintillation vial, 5-bromopicolinic acid (1.0 equiv) and HATU (1.1 equiv) were combined in DMF (0.25 M). *N*,*N*-Diisopropylethylamine (DIPEA, 5 equiv) was then added. After the reaction mixture was stirred for 10 min, the desired amine was added, and the reaction was stirred until determined to be complete by LC−MS (2−20 h). The reaction mixture was filtered through a Fisherbrand Nylon 0.45 μm syringe filter and purified directly by preparative RP-HPLC eluting with 0.1% TFA in H_2O/MeCN (10−90% MeCN).

In a scintillation vial, the aryl bromide (1 equiv), $PdCl_2(PPh_3)_2$ (0.05 equiv), and CuI (0.1 equiv) were combined, placed under argon atmosphere, and dissolved in DMF (0.25M). The desired ethynylpyridine (2- or 4-ethynylpyridine) (1.25 equiv) was added, followed by Et_2NH (6 equiv). The reaction mixture heated to 90 °C for 45 min after which the reaction was determined to be complete by LC−MS. The reaction mixture was filtered through a Fisherbrand Nylon 0.45 μm syringe filter and purified directly by preparative RP-HPLC eluting with 0.1% TFA in H_2O/MeCN (10−90% MeCN) to yield products **44a−d** and **45**.

(*R*)-*N*-(3-Methylbutan-2-yl)-5-(pyridin-2-ylethynyl)-picolinamide (44b). LC−MS: t_R = 0.727 min, >98% at 215 and 254 nm, m/z = 294.2 [M + H]$^+$. $[\alpha]^{20}_D$ = −50.0 (*c* 0.78, $CHCl_3$); ^{1}H NMR (400 MHz, $CDCl_3$) δ 8.72 (1H, d, *J* = 1.7 Hz), 8.65 (1H, d, *J* = 4.7 Hz), 8.20 (1H, d, *J* = 8.1 Hz), 8.00 (1H, dd, *J* = 6.1, 2.0 Hz), 7.89 (1H, d, *J* = 9.0 Hz), 7.73 (1H, dt, *J* = 7.7, 1.6 Hz),), 7.57 (1H, d, *J* = 7.8 Hz), 7.30 (1H, m), 4.05 (1H, m), 1.84 (1H, sep, *J* = 6.5 Hz), 1.21 (3H, d, *J* = 6.7 Hz), 0.97 (6H, dd, *J* = 6.8, 4.0 Hz); ^{13}C NMR (100 MHz, $CDCl_3$) δ 162.8, 150.7, 150.2, 149.1, 142.4, 140.1, 136.3, 127.4, 123.4, 121.7, 121.6, 93.3, 85.1, 50.2, 33.1, 18.6, 18.5, 17.6; HRMS (ES+, M + H) calcd for $C_{18}H_{20}N_3O$ 294.1606, found 294.1607.

(*R*)-*N*-(3-Fluoro-3-methylbutan-2-yl)-5-(pyridin-2-ylethynyl)-picolinamide (44c). (*R*)-*N*-(3-Hydroxy-3-methylbutan-2-yl)-5-(pyridin-2-ylethynyl)picolinamide, **31i**, (39 mg, 0.12 mmol, 1.0 equiv) was dissolved in CH_2Cl_2 (1.2 mL, 0.1 M) and cooled to −78 °C. DAST (19 μL, 0.12 mmol, 1.0 equiv) was added dropwise, and the reaction was allowed to slowly warm to rt over 4 h. The reaction was determined to be complete by LC−MS and was quenched carefully by the addition of H_2O (0.5 mL). The aqueous layer was extracted with EtOAc (3 × 5 mL), dried Na_2SO_4, concentrated, and purified by preparative RP-HPLC eluting with 0.1% TFA in H_2O/MeCN (10−90% MeCN) to afford the title compound in 81% yield. LC−MS: t_R = 0.671 min, >98% at 215 and 254 nm, m/z = 312.2 [M + H]$^+$. $[\alpha]^{20}_D$ = −14.0 (*c* 0.46, $CHCl_3$); ^{1}H NMR (400 MHz, $CDCl_3$) δ 8.75 (1H, dd, *J* = 1.9, 0.6 Hz), 8.67 (1H, d, *J* = 4.0 Hz), 8.20 (1H, dd, *J* = 8.1, 0.6 Hz), 8.15 (1H, d, *J* = 9.8 Hz), 8.02 (1H, dd, *J* = 8.1, 2.0 Hz), 7.74 (1H, dt, *J* = 7.8, 1.8 Hz), 7.58 (1H, d, *J* = 7.8 Hz), 7.31 (1H, m), 4.28 (1H, m), 1.45 (3H, d, *J* = 16.2 Hz), 1.45 (3H, d, *J* = 16.4 Hz), 1.45 (3H, d, *J* = 6.9 Hz); ^{13}C NMR (100 MHz, $CDCl_3$) δ 163.0, 150.8, 150.3, 148.7, 142.4, 140.1, 136.3, 127.4, 123.5, 122.0, 121.7, 96.5 (d, J_{C-F} = 170.8 Hz), 93.5, 84.8, 51.4 (d, J_{C-F} = 22.3 Hz), 24.5 (d, J_{C-F} = 5.8 Hz), 24.2 (d, J_{C-F} = 5.3 Hz), 15.5 (d, J_{C-F} = 3.8 Hz); HRMS (ES+, M + H) calcd for $C_{18}H_{19}FN_3O$ 312.1512, found 312.1511.

***N*-(3-Methyloxetan-3-yl)-5-(pyridin-2-ylethynyl)-picolinamide (44d).** LC−MS: t_R = 0.453 min, >98% at 215 and 254 nm, m/z = 294.2 [M + H]$^+$. ^{1}H NMR (400 MHz, $CDCl_3$) δ 8.72 (1H, d, *J* = 1.2 Hz), 8.66 (1H, d, *J* = 4.4 Hz), 8.28 (1H, bs), 8.15 (1H, d, *J* = 8.1 Hz), 8.02 (1H, dd, *J* = 9.2, 3.0 Hz), 7.73 (1H, td, *J* = 7.8, 1.6 Hz), 7.58 (1H, d, *J* = 7.8 Hz), 7.31 (1H, m), 4.94 (2H, d, *J* = 6.3 Hz), 4.58 (2H, d, *J* = 6.5 Hz), 1.77 (3H, s); ^{13}C NMR (100 MHz, $CDCl_3$) δ 162.9, 150.8, 150.3, 148.6, 142.4, 140.3, 136.4, 127.4, 123.6, 122.4, 121.4, 93.7, 84.9, 81.9, 53.7, 23.7; HRMS (ES+, M + H) calcd for $C_{17}H_{16}N_3O_2$ 294.1243, found 294.1240.

***N*-(3-Methyloxetan-3-yl)-5-(pyridin-4-ylethynyl)-picolinamide (45).** LC−MS: t_R = 0.354 min, >98% at 215 and 254 nm, m/z = 294.2 [M + H]$^+$. ^{1}H NMR (400 MHz, $CDCl_3$) δ 8.67 (1H, d, *J* = 1.2 Hz), 8.65 (2H, m), 8.29 (1H, bs), 8.16 (1H, d, *J* = 8.1 Hz),

7.98 (1H, dd, J = 8.1, 1.9 Hz), 7.41 (2H, d, J = 5.6 Hz), 4.93 (2H, d, J = 6.4 Hz), 4.58 (2H, d, J = 6.4 Hz), 1.77 (3H, s); ^{13}C NMR (100 MHz, $CDCl_3$) δ 162.9, 150.5, 149.9, 148.8, 140.1, 130.2, 125.5, 122.0, 121.4, 91.7, 89.5, 81.8, 53.7, 23.6; HRMS (ES+, M + H) calcd for $C_{17}H_{16}N_3O_2$ 294.1243, found 294.1242.

Fluorescence-Based Calcium Flux Assay (Concentration−Response Curve (Potency) and Glutamate Fold Shift (Efficacy). For measurement of compound-evoked increases in intracellular calcium, HEK293 cells stably expressing rat $mGlu_5$ were plated in 384-well,[44] poly-D-lysine coated, black-walled, clear-bottomed plates in 20 μL of assay medium (DMEM supplemented with 10% dialyzed fetal bovine serum, 20 mM HEPES, and 1 mM sodium pyruvate) at a density of 15,000 cells/well. Cells were grown overnight at 37 °C/5% CO_2. The next day, medium was removed from the cells, and they were incubated with 20 μL/well of 1 μM Fluo-4AM (Invitrogen, Carlsbad, California) prepared as a 2.3 mM stock in dimethyl sulfoxide (DMSO) and mixed in a 1:1 ratio with 10% (w/v) pluronic acid F-127 and diluted in calcium assay buffer (Hank's Balanced Salt Solution (HBSS; Invitrogen, Carlsbad, CA) supplemented with 20 mM HEPES and 2.5 mM probenecid, pH 7.4) for 50 min at 37 °C. Dye loading solution was removed and replaced with 20 μL/well of assay buffer. For PAM potency curves, $mGlu_5$ compounds were diluted in calcium assay buffer and added to the cells followed by the addition of an EC_{20} concentration of glutamate 140 s later and then an EC_{80} concentration of glutamate 60 s later. For fold-shift experiments either a single concentration (10 μM) or multiple fixed concentrations (50 nM to 30 μM) of $mGlu_5$ compound or vehicle were added followed by the addition of a concentration−response curve (CRC) of glutamate 140 s later. Calcium flux was measured over time as an increase in fluorescence using a Functional Drug Screening System 6000 (FDSS 6000, Hamamatsu, Japan). The change in relative fluorescence over basal was calculated before normalization to the maximal response to glutamate.

Selectivity Screening. $mGlu_1$. To assess the effect of test compounds at $mGlu_1$, Ca^{2+} mobilization assays were performed as described previously.[35,43] Briefly HEK293 cells stably expressing rat $mGlu_1$ were plated in black-walled, clear-bottomed, poly-D-lysine-coated 384-well plates (Greiner Bio-One, Monroe, NC) in assay medium at a density of 20,000 cells/well. Calcium flux was measured over time as an increase in fluorescence of the Ca^{2+} indicator dye Fluo-4AM using a FDSS 6000. Either vehicle or a fixed concentration of test compound (10 μM, final concentration) was added followed 140 s later by a CRC of glutamate. Data were analyzed as described above.

Group II and Group III mGlus. The functional activity of the compounds of interest was assessed at the rat group II and III mGlu receptors by measuring thallium flux through GIRK channels as previously described.[61] Briefly, HEK293-GIRK cells expressing mGlu subtypes 2, 3, 4, 6, 7, or 8 were plated into 384-well, black-walled, clear-bottom poly-D-lysine coated plates at a density of 15,000 cells/well in assay medium. A single concentration of test compound (10 μM) or vehicle was added followed 140 s later by a CRC of glutamate (or L-AP4 for $mGlu_7$) diluted in thallium buffer (125 mM $NaHCO_3$, 1 mM $MgSO_4$, 1.8 mM $CaSO_4$, 5 mM glucose, 12 mM thallium sulfate, 10 mM HEPES), and fluorescence was measured using a FDSS 6000. Data were analyzed as described previously.[61]

Radioligand Binding. Membranes were prepared from HEK293A cells expressing rat $mGlu_5$. Cells were harvested and pelleted by centrifugation, resuspended in ice-cold homogenization buffer (50 mM Tris-HCl, 10 mM EDTA, 0.9% NaCl, pH7.4), and homogenized by 3 × 10 s bursts. Cell fractions were separated by centrifugation, and the resulting pellet resuspended in ice-cold assay buffer (50 mM Tris-HCl, 0.9% NaCl, pH7.4). For inhibition binding experiments, membranes (50 μg/well) were incubated with 7 nM [^{3}H]methoxyPEPy and a range of concentrations of test ligand for 1 h at room temperature with shaking in assay buffer. Ten micromolar MPEP was used to determine nonspecific binding. Assays were terminated by rapid filtration using a Brandel 96-well plate Harvester and washed three times with ice-cold assay buffer. The next day MicroScint20 was added, and radioactivity was counted.

Electrophysiology (LTD and Epileptiform Studies). All animals used in these studies were cared for in accordance with the NIH Guide for the Care and Use of Laboratory Animals. Either 30−40 (LTD experiments) or 24−30 (epileptiform experiments) day old male Sprague−Dawley rats were used. The brains were quickly removed and submerged into ice-cold cutting solution (in mM: 110 sucrose, 60 NaCl, 3 KCl, 1.25 NaH_2PO_4, 28 $NaHCO_3$, 5 glucose, 0.6 (+)-sodium-L-ascorbate, 0.5 $CaCl_2$, 7 $MgCl_2$). All solutions were continuously bubbled with 95% O_2/5% CO_2. Transverse slices (400 μm) were made using a vibratome (Leica VT100S). For LTD experiments, individual hippocampi were microdissected out, transferred to a room temperature mixture containing equal volumes of cutting solution and artificial cerebrospinal fluid (ACSF; in mM: 125 NaCl, 2.5 KCl, 1.25 NaH_2PO_4, 25 $NaHCO_3$, 25 glucose, 2 $CaCl_2$, 1 $MgCl_2$), and equilibrated for 30 min, followed by room temperature ACSF for 1 h. For epileptiform experiments, individual hippocampi were transferred directly into room temperature ACSF (in mM: 124 NaCl, 5 KCl, 1.25 NaH_2PO_4, 26 $NaHCO_3$, 10 glucose, 2 $CaCl_2$, 1.2 $MgSO_4$) and equilibrated for 1 h. Slices were transferred to a submersion recording chamber and equilibrated for 5−10 min at 30−32 °C. A bipolar-stimulating electrode was placed in the stratum radiatum near the CA3-CA1 border in order to stimulate the Schaffer collaterals. Recording electrodes were filled with ACSF and placed in the stratum radiatum of area CA1 (LTD experiments) or in the pyramidal cell body layer of CA3 (epileptiform experiments). Field potential recordings were acquired using a Multiclamp 700B (Warner Instruments) amplifier and pClamp 9.2 software. For stimulation-based experiments an intensity that produced 50−60% of the maximum was used as the baseline stimulation. $mGlu_5$ compounds were diluted to the appropriate concentrations in DMSO and applied to the bath using a perfusion system. Sampled data was analyzed by averaging three sequential field excitatory postsynaptic potentials (fEPSPs) slopes, followed by normalizing to the average slope calculated during the predrug period (percent of baseline). For epileptiform experiments, spontaneous events were measured using MiniAnalysis (Synaptosoft Inc., NJ), and inter-event interval (IEI) was normalized to the baseline response.

Comparative Modeling of receptor. The comparative model of $mGlu_5$ was constructed as described previously.[47] In brief, the X-ray crystal structure for human β2-adrenergic receptor (PDB ID: 2RH1)[49] was chosen as a template on the basis of its high sequence similarity to $mGlu_5$. A profile to profile sequence alignment of TM regions between Class C hepta-helical transmembrane regions and Class A crystal structure templates was directly adopted from Muhlemann et al.,[50] with the exception of TM2, TM4, and TM7, which were based on the alignment of CaSR with Class A hepta-helical regions.[51] The sequence alignment was used to thread the amino acid sequence of the $mGlu_5$ transmembrane helical region onto the backbone coordinates of the β2-adrenergic receptor. The protein structure prediction software package Rosetta 3.4[52] was used to rebuild the loop regions between the helices using Monte Carlo Metropolis (MCM) fragment replacement combined with cyclic coordinate descent loop closure (CCD).[53,54] The resulting full sequence models were then subjected to eight iterative cycles of side chain repacking and gradient minimization of ϕ, ψ, and χ angles in Rosetta Membrane.[55] Over 5,000 comparative models of $mGlu_5$ were generated and clustered for structural similarity using bcl::Cluster.[56] The lowest energy model from the largest cluster was used for further ligand docking studies.

Computational Docking of Ligands. Ligands **19**, **38t**, and **31i** were computationally docked into the comparative model of $mGlu_5$ using Rosetta Ligand.[57−59] Each modulator was allowed to sample docking poses in a 5 Å radius centered at the putative binding site for allosteric modulation, determined by the residues known to affect MPEP affinity.[47] Once a binding mode had been determined by the docking procedure, 10 low energy conformations of the ligand created by MOE (Molecular Operating Environment, Chemical Computing Group, Ontario, Canada) were tested within the site. Side-chain rotamers around the ligand were optimized simultaneously in a Monte Carlo minimization algorithm. The energy function used during the docking procedure contains terms for van der Waals attractive and

repulsive forces, hydrogen bonding, electrostatic interactions between pairs of amino acids, solvation, and a statistical term derived from the probability of observing a side-chain conformation from the Protein Data Bank. For each modulator, over 5,000 docked complexes were generated and clustered for structural similarity using bcl::Cluster.[57] The lowest energy binding mode from the two largest clusters for each modulator, encompassing ligand positions for which the eastern amide was pointing either toward or away from the extracellular surface, were used for further analysis.

■ ASSOCIATED CONTENT

Supporting Information

mGlu selectivity for **38t**, progressive glutamate fold-shift analysis, pK_B and log β calculations, DMPK procedures, compound characterization, and NMR data for compounds. This material is available free of charge via the Internet at http://pubs.acs.org.

■ AUTHOR INFORMATION

Corresponding Author

*Tel: 615-936-8407. E-mail: shaun.stauffer@vanderbilt.edu.

Notes

The authors declare no competing financial interest.

■ ACKNOWLEDGMENTS

Funding for E.D.N. is provided by Public Health Service award T32 GM07347 from the National Institute of General Medical Studies for the Vanderbilt Medical-Scientist Training Program (MSTP) and the Paul Calabresi Medical Student Research Fellowship from the Pharmaceutical Research and Manufacturers of America (PhRMA) Foundation. This work was supported in part by grants from the NIH (NS031373 and MH062646). Vanderbilt is a member of the MLPCN and houses the Vanderbilt Specialized Chemistry Center for Accelerated Probe Development (U54MH084659).

■ ABBREVIATIONS USED

mGlu, metabotropic glutamate receptor; PAM, positive allosteric modulator; NAM, negative allosteric modulator; SAM, silent allosteric modulator; PCP, phenylcyclidene; NMDAR, ionotropic *N*-methyl-D-aspartate glutamate receptor; DHPG, dihydroxyphenylglycine; LTD, long-term depression; MTEP, 3-((2-methyl-4-thiazolyl)ethynyl)pyridine; MPEP, 2-methyl-6-(phenylethynyl)pyridine; DFB, 3,3′-difluorobenzaldazine; CPPHA, *N*-(4-chloro-2-((1,3-dioxoisoindolin-2-yl)-methyl)phenyl)-2-hydroxybenzamide; CDPPB, 3-cyano-*N*-(1,3-diphenyl-1*H*-pyrazol-5-yl)benzamide; AHL, amphetamine-induced hyperlocomotion; MWM, Morris water maze; MAM, methylazoxymethanol; EEG, electroencephalogram; DMTP, delayed-matching-to-position; MLPCN, molecular libraries probe production centers network

■ REFERENCES

(1) Chavez-Noriega, L. E.; Marino, M. J.; Schaffhauser, H.; Campbell, U. C.; Conn, P. J. Novel potential therapeutics for schizophrenia: Focus on the modulation of metabotropic glutamate receptor function. *Curr. Neuropharm.* **2005**, *3*, 9−34.

(2) Lindsley, C. W.; Shipe, W. D.; Wolkenberg, S. E.; Theberge, C. R.; Williams, D. L., Jr.; Sur, C.; Kinney, G. G. Progress towards validating the NMDA receptor hypofunction hypothesis of schizophrenia. *Curr. Top. Med. Chem.* **2006**, *6*, 771−785.

(3) Lisman, J. E.; Coyle, J. T.; Green, R. W.; Javitt, D. C.; Benes, F. M.; Heckers, S.; Grace, A. A. Circuit-based framework for understanding neurotransmitter and risk gene interactions in schizophrenia. *Trends Neurosci.* **2008**, *31*, 234−242.

(4) Conn, P. J.; Lindsley, C. W.; Jones, C. K. Activation of metabotropic glutamate receptors as a novel approach for the treatment of schizophrenia. *Trends Pharmacol. Sci.* **2009**, *30*, 25−31.

(5) Toda, M.; Abi-Dargham, A. Dopamine hypothesis of schizophrenia: making sense of it all. *Curr. Psychiatry Rep.* **2007**, *9*, 329−336.

(6) Stahl, S. M. Beyond the dopamine hypothesis to the NMDA glutamate receptor hypofunction hypothesis of schizophrenia. *CNS Spectrums* **2007**, *12*, 265−268.

(7) Stargardt, T.; Weinbrenner, S.; Busse, R.; Juckel, G.; Gericke, C. A. Effectiveness and cost of atypical versus typical antipsychotic treatment for schizophrenia in routine care. *J. Ment. Health Policy Econ.* **2008**, *11*, 89−97.

(8) Crossley, N. A.; Constante, M.; McGuire, P.; Power, P. Efficacy of atypical v. typical antipsychotics in the treatment of early psychosis: meta-analysis. *Br. J. Psychiatry* **2010**, *196*, 434−439.

(9) Coyle, J. T. Glutamate and schizophrenia: beyond the dopamine hypothesis. *Cell. Mol. Neurobiol.* **2006**, *26*, 365−384.

(10) Lewis, D. A.; Moghaddam, B. Cognitive dysfunction in schizophrenia: convergence of gamma-aminobutyric acid and glutamate alterations. *Arch. Neurol.* **2006**, *63*, 1372−1376.

(11) Carlsson, A. The neurochemical circuitry of schizophrenia. *Pharmacopsychiatry* **2006**, *39*, S10−S14.

(12) Marek, G. J.; Behl, B.; Bespalov, A. Y.; Gross, G.; Lee, Y.; Schoemaker, H. Glutamatergic (*N*-methyl-D-aspartate receptor) hypofrontality in schizophrenia: too little juice or a miswired brain? *Mol. Pharmacol.* **2010**, *77*, 317−326.

(13) Niswender, C. M.; Conn, J. P. Metabotropic glutamate receptors: Physiology, pharmacology, and disease. *Annu. Rev. Pharmacol. Toxicol.* **2010**, *50*, 295−322.

(14) Heresco-Levy, U.; Ermilov, M.; Shimoni, J.; Shapira, B.; Silipo, G.; Javitt, D. C. Placebo-controlled trial of D-cycloserine added to conventional neuroleptics, olanzapine, or risperidone in schizophrenia. *Am. J. Psychiatry* **2002**, *159*, 480−482.

(15) Javitt, D. C.; Silipo, G.; Cienfeugos, A.; Shelley, A. M.; Bark, N.; Park, M.; Lindenmayer, J. P.; Suckow, R.; Zukin, S. R. Adjunctive high-dose glycine in the treatment of schizophrenia. *Int. J. Neuropsychopharmacol.* **2001**, *4*, 385−391.

(16) Lindsley, C. W.; Stauffer, S. R. Metabotropic glutamate receptor 5-positive allosteric modulators for the treatment of schizophrenia (2004−2012). *Pharm. Pat. Anal.* **2013**, *2*, 93−108.

(17) Stauffer, S. R. Progress toward positive allosteric modulators of the metabotropic glutatamate receptor subtype 5 ($mGlu_5$). *ACS Chem. Neurosci.* **2011**, *2*, 450−470.

(18) Bridges, T. M.; Lindsley, C. W. G-protein-coupled receptors: from classical modes of modulation to allosteric mechanisms. *ACS Chem. Biol.* **2008**, *3*, 530−541.

(19) Conn, P. J.; Christopoulos, A.; Lindsley, C. W. Allosteric modulators of GPCRs: a novel approach for the treatment of CNS disorders. *Nat. Rev. Drug Discovery* **2009**, *8*, 41−54.

(20) Melancon, B. J.; Hopkins, C. R.; Wood, M. R.; Emmitte, K. A.; Niswender, C. M.; Christopoulos, A.; Conn, P. J.; Lindsley, C. W. Allosteric modulation of seven transmembrane spanning receptors: theory, practice, and opportunities for central nervous system drug discovery. *J. Med. Chem.* **2012**, *55*, 1445−1464.

(21) O'Brien, J. A.; Lemaire, W.; Wittmann, M.; Jacobson, M. A.; Ha, S. N.; Wisnoski, D. D.; Lindsley, C. W.; Schaffhauser, H. J.; Rowe, B.; Sur, C.; Duggan, M. E.; Pettibone, D. J.; Conn, P. J.; Williams, D. L., Jr. A novel selective allosteric modulator potentiates the activity of native metabotropic glutamate receptor subtype 5 in rat forebrain. *J. Pharmacol. Exp. Ther.* **2004**, *309*, 568−577.

(22) Lindsley, C. W.; Wisnoski, D. D.; Leister, W. H.; O'Brian, J. A.; Lemair, W.; Williams, D. L., Jr.; Burno, M.; Sur, C.; Kinney, G. G.; Pettibone, D. J.; Tiller, P. R.; Smith, S.; Duggan, M. E.; Hartman, G. D.; Conn, P. J.; Huff, J. R. Discovery of positive allosteric modulators for the metabotropic glutamate receptor subtype 5 from a series of *N*-

(1,3-diphenyl-1*H*- pyrazol-5-yl)benzamides that potentiate receptor function in vivo. *J. Med. Chem.* **2004**, *47*, 5825−5828.

(23) Kinney, G. G.; O'Brian, J. A.; Lemaire, W.; Burno, M.; Bickel, D. J.; Clements, M. K.; Chen, T. B.; Wisnoski, D. D.; Lindsley, C. W.; Tiller, P. R.; Smith, S.; Jacobson, M. A.; Sur, C.; Duggan, M. E.; Pettibone, D. J.; Conn, P. J.; Williams, D. L., Jr. A novel selective positive allosteric modulator of metabotropic glutamate receptor subtype 5 has in vivo activity and antipsychotic-like effects in rat behavioral models. *Pharamacol. Exp. Ther.* **2005**, *313*, 199−206.

(24) Liu, F.; Grauer, S.; Kelley, C.; Navarra, R.; Graf, R.; Zhang, G.; Atkinson, P. J.; Popiolek, M.; Wantuch, C.; Khawaja, X.; Smith, D.; Olsen, M.; Kouranova, E.; Lai, M.; Pruthi, F.; Pulicicchio, C.; Day, M.; Gilbert, A.; Pausch, M. H.; Brandon, N. J.; Beyer, C. E.; Comery, T. A.; Logue, S.; Rosenzweig-Lipson, S.; Marquis, K. L. ADX47273 [S-(4-fluoro-phenyl)-{3-[3-(4-fluoro-phenyl)-[1,2,4]-oxadiazol-5-yl]-piperidin-1-yl}-methanone]: a novel metabotropic glutamate receptor 5-selective positive allosteric modulator with preclinical antipsychotic-like and procognitive activities. *J. Pharmacol. Exp. Ther.* **2008**, *327*, 827−839.

(25) Spear, N.; Gadient, R. A.; Wilkins, D. E.; Do, M.; Smith, J. S.; Zeller, K. L.; Schroeder, P.; Zhang, M.; Arora, J.; Chhajlani, V. Preclinical profile of a novel metabotropic glutamate receptor 5 positive allosteric modulator. *Eur. J. Pharmacol.* **2011**, *659*, 146−154.

(26) Packiarajan, M.; Mazza Ferreira, C. G.; Hong, S. P.; White, A. D.; Chandrasena, G.; Pu, X.; Brodbeck, R. M.; Robichaud, A. J. *N*-Aryl pyrrolidinonyl oxadiazoles as potent mGlu5 positive allosteric modulators. *Bioorg. Med. Chem. Lett.* **2012**, *22*, 5658−5662.

(27) Packiarajan, M.; Ferreira, C. G.; Hong, S. P.; White, A. D.; Chandrasena, G.; Pu, X.; Brodbeck, R. M.; Robichaud, A. J. Azetidinyl oxadiazoles as potent mGlu5 positive allosteric modulators. *Bioorg. Med. Chem. Lett.* **2012**, *22*, 6469−6474.

(28) Gilmour, G.; Broad, L. M.; Wafford, K. A.; Britton, T.; Colvin, E. M.; Fivush, A.; Gastambide, F.; Getman, B.; Heinz, B. A.; McCarthy, A. P.; Prieto, L.; Shanks, E.; Smith, J. W.; Taboada, L.; Edgar, D. M.; Tricklebank, M. D. In vitro characterisation of the novel positive allosteric modulators of the $mGlu_5$ receptor, LSN2463359 and LSN2814617, and their effects on sleep architecture and operant responding in the rat. *Neuropharmacology* **2013**, *64*, 224−239.

(29) Vanejevs, M.; Jatzke, C.; Renner, S.; Müller, S.; Hechenberger, M.; Bauer, T.; Klochkova, A.; Pyatkin, I.; Kazyulkin, D.; Aksenova, E.; Shulepin, S.; Timonina, O.; Haasis, A.; Gutcaits, A.; Parsons, C. G.; Kauss, V.; Weil, T. Positive and negative modulation of group I metabotropic glutamate receptors. *J. Med. Chem.* **2008**, *51*, 634−647.

(30) Sharma, S.; Kedrowski, J.; Rook, J. M.; Smith, R. L.; Jones, C. K.; Rodriguez, A. L.; Conn, P. J.; Lindsley, C. W. Discovery of molecular switches that modulate modes of metabotropic glutamate receptor subtype 5 (mGlu5) pharmacology in vitro and in vivo within a series of functionalized, regioisomeric 2- and 5-(phenylethynyl)pyrimidines. *J. Med. Chem.* **2009**, *52*, 4103−4106.

(31) Ritzén, A.; Sindet, R.; Hentzer, M.; Svendsen, N.; Brodbeck, R. M.; Bundgaard, C. Discovery of a potent and brain penetrant mGlu5 positive allosteric modulator. *Bioorg. Med. Chem. Lett.* **2009**, *19*, 3275−3278.

(32) Varnes, J. G.; Marcus, A. P.; Mauger, R. C.; Throner, S. R.; Hoesch, V.; King, M. M.; Wang, X.; Sygowski, L. A.; Spear, N.; Gadient, R.; Brown, D. G.; Campbell, J. B. Discovery of novel positive allosteric modulators of the metabotropic glutamate receptor 5 (mGlu5). *Bioorg. Med. Chem. Lett.* **2011**, *21*, 1402−1406.

(33) Bartolomé-Nebreda, J. M.; Conde-Ceide, S.; Delgado, F.; Iturrino, L.; Pastor, J.; Pena, M. A.; Trabanco, A. A.; Tresadern, G.; Wassvik, C. M.; Stauffer, S. R.; Jadhav, S.; Gogi, K.; Vinson, P. N.; Days, E.; Weaver, C. D.; Lindsley, C. W.; Niswender, C. M.; Jones, C. K.; Conn, P. J.; Rombouts, F.; Lavreysen, H.; Macdonald, G. J.; Mackie, C.; Steckler, T. Dihydrothiazolopyridone derivatives as a novel family of positive allosteric modulators of the mGlu5 receptor. *J. Med. Chem.* **2013**, *56*, 7243−7259.

(34) Manka, J. T.; Vinson, P. N.; Gregory, K. J.; Zhou, Y.; Williams, R.; Gogi, K.; Days, E.; Jadhav, S.; Herman, E. J.; Lavreysen, H.; Mackie, C.; Bartolomé, J. M.; MacDonald, G. J.; Steckler, T.; Daniels, J. S.; Weaver, C. D.; Niswender, C. M.; Jones, C. K.; Conn, P. J.; Lindsley, C. W.; Stauffer, S. R. Optimization of an ether series of mGlu5 positive allosteric modulators: molecular determinants of MPEP-site interaction crossover. *Bioorg. Med. Chem. Lett.* **2012**, *22*, 6481−6485.

(35) Hammond, A. S.; Rodriguez, A. L.; Townsend, S. D.; Niswender, C. M.; Gregory, K. J.; Lindsley, C. W.; Conn, P. J. Discovery of a novel chemical class of mGlu(5) allosteric ligands with distinct modes of pharmacology. *ACS Chem. Neurosci.* **2010**, *1*, 702−716.

(36) Ayala, J. E.; Chen, Y.; Banko, J. L.; Sheffler, D. J.; Williams, R.; Telk, A. N.; Watson, N. L.; Xiang, Z.; Zhang, Y.; Jones, P. J.; Lindsley, C. W.; Olive, M. F.; Conn, P. J. mGlu5 positive allosteric modulators facilitate both hippocampal LTP and LTD and enhance spatial learning. *Neuropsychopharmacology* **2009**, *34*, 3057−3071.

(37) Rook, J. M.; Noetzel, M. J.; Pouliot, W. A.; Bridges, T. M.; Vinson, P. N.; Cho, H. P.; Zhou, Y.; Gogliotti, R. D.; Manka, J. T.; Gregory, K. J.; Stauffer, S. R.; Dudek, F. E.; Xiang, Z.; Niswender, C. M.; Daniels, J. S.; Jones, C. K.; Lindsley, C. W.; Conn, P. J. Unique signaling profiles of positive allosteric modulators of metabotropic glutamate receptor subtype 5 determine differences in in vivo activity. *Biol. Psychiatry* **2013**, *73*, 501−509.

(38) Bridges, T. M.; Rook, J. M.; Noetzel, M. J.; Morrison, R. D.; Zhou, Y.; Gogliotti, R. D.; Vinson, P. N.; Jones, C. K.; Niswender, C. M.; Lindsley, C. W.; Stauffer, S. R.; Conn, P. J.; Daniels, J. S. Biotransformation of a novel positive allosteric modulator of metabotropic glutamate receptor subtype 5 contributes to seizure-like adverse events in rats involving a receptor agonism-dependent mechanism. *Drug Metab. Dispos.* **2013**, *41*, 703−714.

(39) Parmentier-Batteur, S.; Hutson, P. H.; Menzel, K.; Uslaner, J. M.; Mattson, B. A.; O'Brien, J. A.; Magliaro, B. C.; Forest, T.; Stump, C. A.; Tynebor, R. M.; Anthony, N. J.; Tucker, T. J.; Zhang, X. F.; Gomez, R.; Huszar, S. L.; Lambeng, N.; Fauré, H.; Le Poul, E.; Poli, S.; Rosahl, T. W.; Rocher, J. P.; Hargreaves, R.; Williams, T. M. Mechanism based neurotoxicity of mGlu5 positive allosteric modulators—Development challenges for a promising novel antipsychotic target. *Neuropharmacology* **2013**, DOI: 10.1016/j.neuropharm.2012.12.003.

(40) Merlin, L. R.; Wong, R. K. Role of group I metabotropic glutamate receptors in the patterning of epileptiform activities in vitro. *J. Neurophysiol.* **1997**, *78*, 539−44.

(41) Wong, R. K.; Bianchi, R.; Chuang, S. C.; Merlin, L. R.; Group, I. mGlu-induced epileptogenesis: distinct and overlapping roles of mGlu1 and mGlu5 and implications for antiepileptic drug design. *Epilepsy Curr.* **2005**, *5*, 63−68.

(42) Rodriguez, A. L.; Grier, M. D.; Jones, C. K.; Herman, E. J.; Kane, A. S.; Smith, R. L.; Williams, R.; Zhou, Y.; Marlo, J. E.; Days, E. L.; Blatt, T. N.; Jadhav, S.; Menon, U. N.; Vinson, P. N.; Rook, J. M.; Stauffer, S. R.; Niswender, C. M.; Lindsley, C. W.; Weaver, C. D.; Conn, P. J. Discovery of novel allosteric modulators of metabotropic glutamate receptor subtype 5 reveals chemical and functional diversity and in vivo activity in rat behavioral models of anxiolytic and antipsychotic activity. *Mol. Pharmacol.* **2010**, *78*, 1105−1123.

(43) Noetzel, M. J.; Rook, J. M.; Vinson, P. N.; Cho, H. P.; Days, E.; Zhou, Y.; Rodriguez, A. L.; Lavreysen, H.; Stauffer, S. R.; Niswender, C. M.; Xiang, Z.; Daniels, J. S.; Jones, C. K.; Lindsley, C. W.; Weaver, C. D.; Conn, P. J. Functional impact of allosteric agonist activity of selective positive allosteric modulators of metabotropic glutamate receptor subtype 5 in regulating central nervous system function. *Mol. Pharmacol.* **2012**, *81*, 120−133.

(44) Sams, A. G.; Mikkelsen, G. K.; Brodbeck, R. M.; Pu, X.; Ritzén, A. Efficacy switching SAR of mGlu5 allosteric modulators: highly potent positive and negative modulators from one chemotype. *Bioorg. Med. Chem. Lett.* **2011**, *21*, 3407−3410.

(45) (a) Wuitschik, G.; Carreira, E. M.; Wanger, B.; Fischer, H.; Parrilla, I.; Schuler, F.; Rogers-Evans, M.; Müller, K. Oxetanes in drug discovery: Structural and synthetic insights. *J. Med. Chem.* **2010**, *53*, 3227−3246. (b) Burkhard, J. A.; Wuitschik, G.; Rogers-Evans, M.;

Müller, K.; Carreira, E. M. Oxetanes as versatile elements in drug discovery and synthesis. *Angew. Chem., Int. Ed.* **2010**, *49*, 9052−9067.
(46) Gregory, K. J.; Noetzel, M. J.; Rook, J. M.; Vinson, P. N.; Stauffer, S. R.; Rodriguez, A. L.; Emmitte, K. A.; Zhou, Y.; Chun, A. C.; Felts, A. S.; Chauder, B. A.; Lindsley, C. W.; Niswender, C. M.; Conn, P. J. Investigating metabotropic glutamate receptor 5 allosteric modulator cooperativity, affinity, and agonism: enriching structure-function studies and structure-activity relationships. *Mol. Pharmacol.* **2012**, *82*, 860−875.
(47) Gregory, K. J.; Nguyen, E. D.; Reiff, S. D.; Squire, E. F.; Stauffer, S. R.; Lindsley, C. W.; Meiler, J.; Conn, P. J. Probing the metabotropic glutamate receptor 5 (mGlu5) positive allosteric modulator (PAM) binding pocket: Discovery of point mutations that engender a "molecular switch" in PAM pharmacology. *Mol. Pharmacol.* **2013**, *83*, 991−1006.
(48) Merlin, L. R.; Bergold, P. J.; Wang, M.; Wong, R. K. Requirement of protein synthesis for group I mGluR-mediated induction of epileptiform discharges. *J. Neurophysiol.* **1998**, *80*, 989−993.
(49) Cherezov, V.; Rosenbaum, D. M.; Hanson, M. A.; Rasmussen, S. G.; Thain, F. S.; Kobilka, T. S.; Choi, H. J.; Kuhn, P.; Weis, W. I.; Kobilka, B. K.; Stevens, R. C. High-resolution crystal structure of an engineered human 2-adrenergic G protein coupled receptor. *Science* **2007**, *318*, 1258−1265.
(50) Mühlemann, A.; Ward, N. A.; Kratochwil, N.; Diener, C.; Fischer, C.; Stucki, A.; Jaeschke, G.; Malherbe, P.; Porter, R. H. Determination of key amino acids implicated in the actions of allosteric modulation by 3, 3′-difluorobenzaldazine on rat mGlu5 receptors. *Eur. J. Pharmacol.* **2006**, *529*, 95−104.
(51) Miedlich, S. U.; Gama, L.; Seuwen, K.; Wolf, R. M.; Breitwieser, G. E. Homology modeling of the transmembrane domain of the human calcium sensing receptor and localization of an allosteric binding site. *J. Biol. Chem.* **2004**, *279*, 7254−7263.
(52) Leaver-Fay, A.; Tyka, M.; Lewis, S. M.; Lange, O. F.; Thompson, J.; Jacak, R.; Kaufman, K.; Renfrew, P. D.; Smith, C. A.; Sheffler, W.; Davis, I. W.; Cooper, S.; Treuille, A.; Mandell, D. J.; Richter, F.; Ban, Y. E.; Fleishman, S. J.; Corn, J. E.; Kim, D. E.; Lyskov, S.; Berrondo, M.; Mentzer, S.; Popovic, Z.; Havranekk, J. J.; Karanicolas, J.; Das, R.; Miler, J.; Kortemme, T.; Gray, J. J.; Kuhlman, B.; Baker, D.; Bradley, P. ROSETTA3: an object-oriented software suite for the simulation and design of macromolecules. *Methods Enzymol.* **2011**, *487*, 545−574.
(53) Wang, C.; Bradley, P.; Baker, D. Protein-protein docking with backbone flexibility. *J. Mol. Biol.* **2007**, *373*, 503−519.
(54) Canutescu, A. A.; Dunbrack, R. L. Cyclic coordinate descent: a robotics algorithm for protein loop closure. *Protein Sci.* **2009**, *12*, 963−972.
(55) Yarov-Yarovoy, V.; Schonbrun, J.; Baker, D. Multipass membrane protein structure prediction using Rosetta. *Proteins* **2005**, *62*, 1010−1025.
(56) Alexander, N.; Woetzel, N.; Meiler, J. Bcl:: Cluster: A method for clustering biological molecules coupled with visualization in the Pymol Molecular Graphics System. In *1st IEEE International Conference on Computational Advances in Bio and Medical Sciences (ICCABS)*; IEEE: Piscataway, NJ, 2011; pp 13−18.
(57) Meiler, J.; Baker, D. Rosettaligand: Protein-small molecule docking with full side-chain flexibility. *Proteins* **2006**, *65*, 538−548.
(58) Davis, I. W.; Baker, D. RosettaLigand docking with full ligand and receptor flexibility. *J. Mol. Biol.* **2009**, *385*, 381−392.
(59) Lemmon, G.; Meiler, J. Rosetta Ligand docking with flexible XML protocols. *Methods Mol. Biol.* **2012**, *819*, 143−155.
(60) For information on the MLPCN and information on how to request probe compounds, such as ML254, see: http://mli.nih.gov/mli/mlpcn/
(61) Niswender, C. M.; Johnson, K. A.; Luo, Q.; Ayala, J. E.; Kim, C.; Conn, P. J.; Weaver, C. D. A novel assay of Gi/o-linked G protein-coupled receptor coupling to potassium channels provides new insights into the pharmacology of the group III metabotropic glutamate receptors. *Mol. Pharmacol.* **2008**, *73*, 1213−1224.